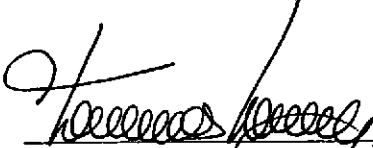
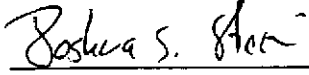


**Analysis Report  
for  
Inclusion of Omitted Areas in Mining Transmissivity  
Calculations  
in Response to EPA Comment G-11**


**(AP-112: Analysis Plan for CRA Response Activities)**

**Task Number 1.2.7  
ERMS #538218**

Author:  Date: 12/20/04  
Thomas S. Lowry, 6115  
Geohydrology Department

Technical Review:  Date: 12/20/2004  
Joshua S. Stein, 6852  
Subsystems Performance Assessment Department

QA Review:  Date: 12/20/2004  
Mario Chavez, 6820  
Carlsbad Programs Group

Management Review:  Date: 12/20/2004  
Mark Rigali, 6822  
Manager, Repository Performance

WIPP:1.2.7:PA:QA-L:Pkg 533999

**Information Only**

# Contents

<b>Table of Contents</b>	<b>2</b>
<b>List of Figures</b>	<b>3</b>
<b>List of Tables</b>	<b>6</b>
<b>1 Introduction</b>	<b>7</b>
1.1 Purpose . . . . .	8
1.2 Outline . . . . .	9
<b>2 Approach</b>	<b>10</b>
2.1 Overview . . . . .	10
2.2 Software . . . . .	11
2.3 File Naming Convention . . . . .	13
2.4 Model Domain and Discretization . . . . .	14
2.5 Boundary and Initial Conditions . . . . .	17
2.6 Subtask 1: Determination of Potential Mining Areas . . . . .	23
2.7 Subtask 2: Use of Mining Zones in Forward Simulations . . . . .	27
2.8 Subtask 3: Particle Tracking using DTRKMF . . . . .	27
<b>3 Modeling Assumptions</b>	<b>28</b>
<b>4 Results</b>	<b>29</b>
4.1 Particle Travel Times . . . . .	29
4.2 Travel Direction . . . . .	32
4.3 Extreme Values . . . . .	38
<b>5 Summary</b>	<b>40</b>
<b>Appendices:</b>	<b>50</b>
<b>A. Qualified runs and random mining factors</b>	<b>50</b>

## List of Figures

1	Software and information flow-chart. Elements within the dashed box are part of AP-100. . . . .	13
2	Directory tree of Task 5 files and programs. <i>Note that the subdirectories d01r02 and d01r04 appearing under the R*/full and R*/partial directories represent the first two of 100 subdirectories.</i> . . . . .	15
3	Modeling domain and boundary conditions for the CRA-revised grid configuration. This is the same domain used in the CRA calculations (Lowry, 2003a). The western no-flow boundary coincides with the groundwater divide underneath Nash draw. . . . .	18
4	The CRA-revised full mining zones overlaid with the 1996 CCA (red) and CRA delineations (blue). . . . .	19
5	The CRA-revised partial mining zones overlaid with the 1996 CCA (red) and CRA delineations (blue). . . . .	20
6	Initial heads across modeling domain. . . . .	22
7	Potential potash distribution in regional area. . . . .	24
8	Potential potash distribution within WIPP boundary (red). The repository structure is shown in the center. Coordinates are UTM NAD 27. . . . .	25
9	Cumulative distribution function plot of the full-, partial-, and non-mining scenarios for the CRA-revised calculations. . . . .	29
10	Normalized pore velocities for the full-mining case. Red indicates zones of highest velocity. The black lines show the full-mining zones and the red box is the WIPP LWB. The T-field used to produce the velocity profile is averaged across all T-field/replicate combinations for the full-mining scenario (300 T-fields in total). . . . .	31
11	Cumulative distribution function plot for the CRA-revised calculations of the 3 full-mining scenario replicates as compared to the CRA and CCA full-mining scenarios. An increase in travel time can be seen over the previous calculations. . . . .	33
12	Cumulative distribution function plot for the CRA-revised calculations of the 3 partial-mining scenario replicates as compared to the CRA and CCA partial-mining scenarios. An increase in travel time can be seen over the previous calculations. . . . .	34
13	Particle tracks of the CRA-revised calculations for replicate 1 for the full-mining scenario. . . . .	35

14	Particle tracks of the CRA-revised calculations for replicate 2 for the full-mining scenario. . . . .	35
15	Particle tracks of the CRA-revised calculations for replicate 3 for the full-mining scenario. . . . .	36
16	Particle tracks of the CRA-revised calculations for replicate 1 for the partial-mining scenario. . . . .	36
17	Particle tracks of the CRA-revised calculations for replicate 2 for the partial-mining scenario. . . . .	37
18	Particle tracks of the CRA-revised calculations for replicate 3 for the partial-mining scenario. . . . .	37
19	Correlation between the random mining factor and Log-travel time. . . . .	39
20	Head contours and particle track for the maximum travel time T-field (d22r06-R2) for the full-mining case. The WIPP boundary is the red box in the center of the figure and the particle track is the blue track originating from the approximate center of the WIPP. . . . .	41
21	Head contours and particle track for the minimum travel time T-field (d03r03-R3) for the full-mining case. The WIPP boundary is the red box in the center of the figure and the particle track is the blue track originating from the approximate center of the WIPP. . . . .	42
22	Head contours and particle track for the median travel time T-field (d12r08-R3) for the full-mining case. The WIPP boundary is the red box in the center of the figure and the particle track is the blue track originating from the approximate center of the WIPP. . . . .	43
23	Head contours and particle track for the maximum travel time T-field (d03r01-R3) for the partial-mining case. The WIPP boundary is the red box in the center of the figure and the particle track is the blue track originating from the approximate center of the WIPP. . . . .	44
24	Head contours and particle track for the minimum travel time T-field (d09r06-R2) for the partial-mining case. The WIPP boundary is the red box in the center of the figure and the particle track is the blue track originating from the approximate center of the WIPP. . . . .	45

- 25 Head contours and particle track for the median travel time T-field (d13r07-R2) for the partial-mining case. The WIPP boundary is the red box in the center of the figure and the particle track is the blue track originating from the approximate center of the WIPP. . . . . 46

## List of Tables

1	Modeling software for Task 5. . . . .	11
2	Input and output files used for Task 5. File names in <i>italics</i> denote files associated with Tasks 2 and 3 of AP-100. . . . .	16
3	The coordinates of the corners of the numerical model domain in UTM NAD27 Coordinates. . . . .	21
4	The coordinates of the corners of the WIPP land withdrawal boundary (LWB) in UTM NAD27 Coordinates. . . . .	21
5	Travel time statistics (median, maximum, & minimum) in years for the full and partial mining scenarios as compared to the CRA and non-mining scenarios. . . . .	30

## 1 Introduction

This report addresses comments made by the EPA in response to modeling efforts pertaining to the effects of potash mining on flow and advective transport in the Culebra aquifer. Specifically, it is the response to comment G-11 of the EPA CRA Completeness Report, "Letter to R.P. Detwiler, Acting Manager, Carlsbad Field Office, U.S. Department of Energy from E. Cotsworth, Director, Office of Radiation and Indoor Air, U.S. Environmental Protection Agency, September 2, 2004" (Cotsworth, 2004), which reads:

In section TFIELD-9.1 paragraph 2 of Attachment TFIELD the CRA states: "The current version of the map differs from the one used for the CCA calculations in that several areas north of the LWB have been ruled out as potential mining areas in the updated version due to recent oil and gas drilling in those areas." EPA does not agree with this approach.

In the WIPP Compliance Application Guidance (CAG), we explained that, in implementing this requirement for mining, DOE should examine the "estimated lives of existing mines and plans for new mines in the vicinity of the WIPP" and should "use mineable reserves in estimating mine lives and the extent of potential mining." (See CAG, p. 45) That is, we expected DOE to look broadly at the potential for existing resources to be developed, without substantial deference to whether the leases were currently viable for development. The methodology in the CRA for mining outside the controlled area is inconsistent with this approach. We do not find that the presence of oil or gas drilling is a sufficient basis for eliminating potash mining areas from consideration, especially in light of anecdotal evidence that mining does occur in proximity to such boreholes. DOE must account for the potash mining areas that have been omitted from the current modeling.

In response to comment G-11, we have redefined the mining areas to include all areas of mined and unmined potash resources, including where they fall within 1-mile-radius exclusion zones around oil and gas wells. This new delineation was used for what we designate as the CRA-revised analysis, which is how this current analysis will be addressed throughout this report. Mining calculations done as part of the CRA (Lowry, 2003a) did

not include the 1-mile-radius exclusion zones as part of the potential mining areas and also did not include areas containing potash resources not currently leased. This analysis re-calculates the mining scenarios addressed in the CRA (Lowry, 2003a) using new mining zone delineations that include the areas previously excluded.

## 1.1 Purpose

Potash mining in the WIPP area involves resource extraction below the Culebra dolomite in the underlying McNutt Potash zone, which is part of the larger Salado Formation (Ramsey et al., 1996). It is hypothesized that subsidence of the Culebra due to mining extraction causes fracturing and unconsolidation of the aquifer material that results in higher transmissivities. This increase in transmissivity may significantly change the regional groundwater flow pattern in the Culebra and additionally the transport of any nuclides entering the aquifer from the underlying repository. The purpose of the mining scenario calculations is to determine the impact of potash mining on groundwater flow direction and velocity in the Culebra. Specifically, this analysis involves three subtasks:

1. Update from previous versions (Ramsey et al., 1996; Wallace, 1996; Lowry, 2003a), the potential areas of future potash mining that are within the model domain and map those areas to the new computational grid
2. Modify the calibrated transmissivity fields (T-fields) from Task 4 of AP-088 and Task 1 of AP-100 to include the new mining zones and run steady-state groundwater flow simulations to calculate the new flow-field
3. Perform particle tracking using the new mining-affected flow-fields to determine travel times to the WIPP land-withdrawal boundary (LWB)

This analysis report highlights the differences and additions relative to the “Analysis Package for the Culebra Flow and Transport Calculations (Task 3) of the Performance Assessment Analysis Supporting the Compliance Certification Application” (Ramsey et al., 1996), the “Summary Memo of Record for NS-11; Subsidence Associated with Mining Inside or Outside the Controlled Area” (Wallace, 1996), and “Task 5 of AP-088, Evaluation of Mining



Scenarios” (Lowry, 2003a). Wallace (1996) was required by the EPA pursuant to 40CFR Part 194, which contains the minimum specifications for incorporating potash-mining impacts upon the performance of the WIPP repository. The Summary Memo of Record for NS-11 is the documentation of the efforts to meet regulation 40CFR Part 194 as part of the 1996 certification of the WIPP. The reader is encouraged to review those documents for background information.

## 1.2 Outline

This report documents the data, methods and summary results of the work done in response to EPA comment G-11 of the CRA Completeness Comments, 3rd set, dated September 2, 2004. The sections of this report and a brief description of each subsection are outlined as follows:

### Section 2: Approach

- 2.1: Overview;** Provides an overview and summary of the modeling approach.
- 2.2: Software;** Describes the software usage and information flow between programs.
- 2.3: File Naming Convention;** Describes the file naming conventions and the input and output files for each program.
- 2.4: Modeling Domain and Discretization;** Outlines the computational grid and modeling domain in terms of regional scale coordinates.
- 2.5: Boundary and Initial Conditions;** Describes the determination and justification for the boundary and initial modeling conditions.
- 2.6: Determination of Potential Mining Areas;** Describes the methodology of determining the potential mining areas.
- 2.7: Use of Mining Zones in Forward Simulations;** Describes how mining zones are applied to the flow model.
- 2.8: Particle Tracking using DTRKMF;** Describes the use of the *DTRKMF* particle tracking code.

### Section 3: Modeling Assumptions

Summarizes the major assumptions of Task 5.

### Section 4: Results

Presents results from the Task 5 mining scenario simulations.

## Section 5: Summary

Presents a summary of this entire report.

## 2 Approach

### 2.1 Overview

This analysis (CRA-revised) models two categories of mining-impacted transmissivity fields: one with mining outside the land withdrawal boundary (LWB) only and the other with regions both inside and outside the LWB mined (partial and full-mining scenarios, respectively). Flow modeling is performed starting with 100 stochastically calibrated T-fields from McKenna and Hart (2003b). Each T-field is modified to reflect the effects of mining by multiplying the transmissivity value in cells that lie within designated mining zones by a random factor between 1 and 1000. The range of this factor is set by the EPA in regulation 40CFR Part 194, p. 5229 (Federal Register/vol. 61, No. 28) and is reproduced in Wallace (1996). The scaling factor for each T-field is provided from Latin Hypercube Sampling (LHS).

A forward steady-state flow simulation is run for each new T-field under each mining scenario (full and partial) across three replicates of mining factors, resulting in 600 simulations (there are 100 calibrated T-fields from Task 1 of AP-100). Particle tracking is performed on the modified flow fields to determine the flow path and groundwater travel time from a point above the center of the WIPP disposal panels to the LWB. Cumulative probability distribution functions (CDFs) are produced for each mining scenario and compared to the undisturbed scenario generated from Task 4 of AP-088, as well as to the full- and partial-mining scenarios from the 1996 CCA and the 2004 CRA (Lowry, 2003a). The CDFs describe the probability of a conservative tracer reaching the LWB at a given time. In addition to comparing travel times, particle-tracking directions are also examined to determine the effect on the regional flow direction in the WIPP area due to mining.

The flow fields generated from the mining scenarios are then refined as part of Tasks 2 and 3 of AP-100 (Leigh et al., 2003) and passed to Task 6 of AP-100, which performs radionuclide transport modeling in the Culebra. The detailed steps involved in Tasks 2 and 3 of AP-100 can be found in Lowry (2003b). Their inclusion in this report is only to provide context to the procedures and approach of Task 5.

Table 1: Modeling software for Task 5.

Code Name	Description	ERMS #
<b>MODFLOW 2000, v1.6</b>	Groundwater Flow Model	523867
<b>DTRKMF</b>	Particle-tracking model	523244

## 2.2 Software

The forward steady-state flow modeling is performed using **MODFLOW 2000 (MF2K)**, version 1.6 (Harbaugh et al., 2000). The same executable used for the Task 4 calibration and the CRA mining calculations is used in this analysis. **MF2K** is a modular, finite-difference code for solving the groundwater flow equation on a two- or three-dimensional rectilinear grid. The code **DTRKMF** (Rudeen, 2003) is used to perform the particle-tracking simulations. **DTRKMF** calculates particle tracks in 2-D or 3-D for steady-state and time-dependent, variably saturated flow fields. The particles are tracked cell-by-cell using a semi-analytical solution (WIPP\_PA, 2003). **DTRKMF** assumes that the velocities vary linearly between the cell faces as a function of the space coordinate and, for time-dependent cases, that the velocities at the faces vary linearly between time planes. It directly reads the cell-by-cell flow budget file from **MF2K** and uses those values to calculate the velocity field. The modeling codes for Task 5 are listed in Table (1).

Several FORTRAN utility codes are used for data conversion purposes. These codes are **FM.F**, **PM.F**, **REFINE.F**, **BA.F**, **PTOUT.F**, and **PT-PLOT.F**. Their source codes are reproduced in the Appendices of Lowry (2003a). The first, **FM.F** is the full-mining scenario pre-processor. This code reads in the calibrated T-fields passed from Task 1 of AP-100, as well as the random mining multiplicative factor, multiplies the transmissivity value in the cells that lie within the mining zone areas by the random factor, and then outputs the modified T-field to a file. Likewise, **PM.F** performs the same task but for the partial-mining scenario. **REFINE.F** is specific to Task 2 of AP-100 (Leigh et al., 2003) and converts the calibrated T-field from the 100x100 m uniform cell size (see below) that is used here, to a 50x50 m uniform cell size that is used for Task 6 of AP-100, which performs the radionuclide transport calculations in the mining-affected flow fields using **SECOTP2D**. Output from **REFINE.F** is formatted for input to **MF2K**,

which is then run to provide the cell-by-cell flow budget file on the 50x50 m cell grid. This step is Task 3 of AP-100. **BA.F** is then used to read in the binary budget file from **MF2K** and write it out in ASCII format for porting to a different computer platform via secure FTP for running the **SECOTP2D** simulations. The other two codes, **PTOUT.F** and **PTPLOT.F** are data manipulation codes and are used to convert the **DTRKMF** output to a format that is suitable for summary and visualization.

The Department of Defense Groundwater Modeling System (**GMS**, version 4.0) software is used for digitizing the mining zone areas onto the computational grid as well as for general visualization purposes (**GMS**, 2003). **GMS** is a groundwater modeling and geo-statistical software package that provides a graphical user interface to numerous groundwater modeling codes. Its strength lies in the ability to apply spatially varying data (e.g. the mining zones) to a discrete grid of any given size. **GMS** is not used to perform any calculations or data conversions. Its use in the CRA-revised calculations is to provide visual aid in matching the computational grid to the mining zone map and to perform a coordinate conversion for the mining zone map (see below).

In addition, several Linux shell scripts are used to help automate and coordinate running the programs. Specifically, they are **MINING.SH**, **POST.SH**, and **POST-FLOW.SH**. **MINING.SH** is the main script that coordinates the running of each model and the other scripts in succession. Starting with each replicate directory, **MINING.SH** creates separate directories for the full and partial-mining scenarios, and then under each of those directories, a separate directory for each T-field. The naming convention of the files and T-fields is addressed in Section 2.3. With the directories set-up, **MINING.SH** then calls **FM.F**, **PM.F**, and **REFINE.F** to produce the 100x100 m modified T-fields and the refined 50x50 m modified T-fields, **MF2K** to run the 100x100 m flow model, **DTRKMF** to perform the particle tracking, and then **MF2K** again to run the 50x50 m flow model. Finally **MINING.SH** calls **POST.SH** to gather all the **DTRKMF** output into a single directory called *ptout*, **PTOUT.F** to combine all the **DTRKMF** output into two files (one each for the full and partial-mining scenarios), **BA.F** to convert the binary 50x50 m budget file to ASCII format, and **POST-FLOW.SH** to gather the ASCII budget files into a single directory called *aff*. The shell scripts are reproduced in the Appendices of Lowry (2003a). It should be noted that there are no changes to the FORTRAN utility codes or the shell scripts used in the CRA-revised calculations than those used in

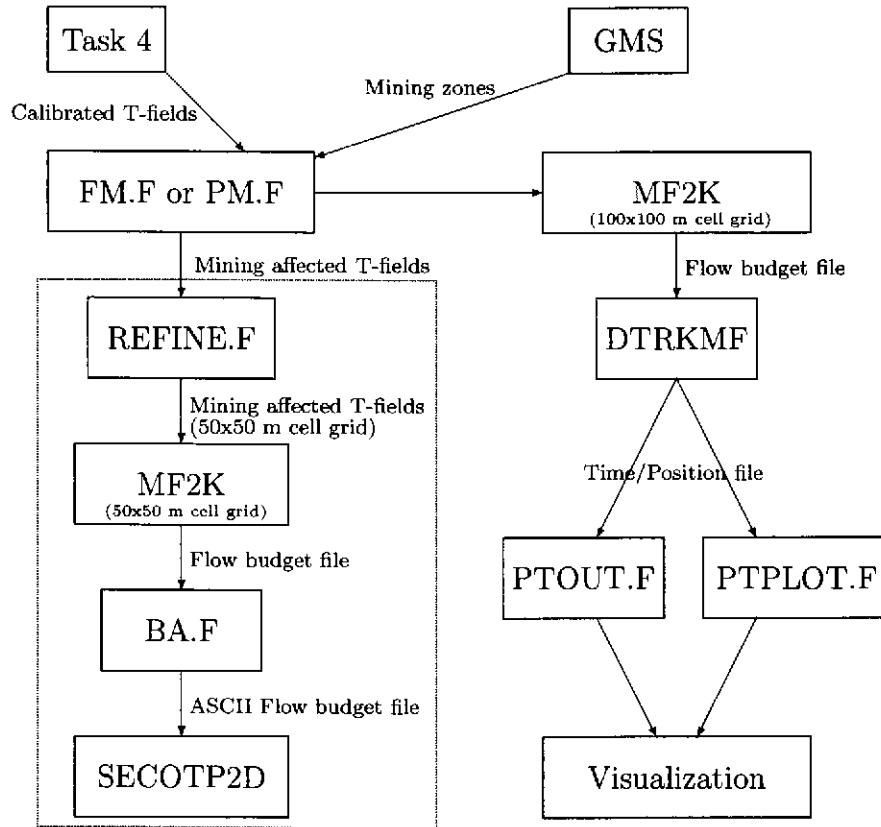


Figure 1: Software and information flow-chart. Elements within the dashed box are part of AP-100.

the CRA calculations (Lowry, 2003a). Copies of these scripts can be found in Lowry (2003a).

Figure (1) shows the software and information flow chart, with the output/input relationship between the different programs.

### 2.3 File Naming Convention

The file naming convention for the CRA-revised calculations are kept consistent with that of Task 4 (McKenna and Hart, 2003b) and the CRA calculations (Lowry, 2003a) to provide continuity between the different analyses. All calculations are performed on the 6115 Linux cluster and are done in a separate directory for each repetition, scenario, and T-field. The general

path for the T-field directories is the same as that of Lowry (2003a) and is:

*/home3/tslowry/wipp/mining/R\*/ [scenario]/d##r##*

where,  $R^*$  is either R1, R2, or R3, depending on the mining factor replicate, *[scenario]* is either 'full' or 'partial', depending on the mining scenario, and *d##r##* is the original base transmissivity field naming convention as described in Holt and Yarbrough (2003). The ##'s next to 'd' ranges from 01 to 22 and next to the 'r' it ranges from 01 to 10. In Task 4 of AP-088, 137 of the 150 calibration runs were successfully calibrated. The 137 successfully calibrated runs were then filtered (Beauheim, 2003) to reduce the number of calibrated fields to 100. Thus for the naming convention, not all values of ## will appear as a directory. In addition, there are two data directories ('100x100' and '50x50') that contain the **MF2K** and **DTRKMF** input files for the 100x100 m and 50x50 m cell grid, respectively, and two directories ('scripts' and 'source') that contain backups of the shell scripts and the FORTRAN source files for the files described above. These directories are subdirectories of */home3/tslowry/wipp/mining*. The parent copy of the shell scripts and the FORTRAN executables are kept in and run from */home3/tslowry/wipp/mining*. A schematic of the directory tree is shown in Figure (2). The input and output files that will remain archived in the directories are listed in Table (2).

## 2.4 Model Domain and Discretization

The model domain used in the CRA-revised analysis is the same as that used in the CRA calculations. A general description of the modeling domain and grid-layout is given in McKenna and Hart (2003a) and is reproduced here for completeness:

The north-south and east-west extent of the model domain was specified by Richard Beauheim, Robert Holt, and Sean McKenna. This determination considered several factors including: 1) hydrogeological features in the vicinity of the WIPP site that could serve as groundwater flow boundaries (e.g. Nash Draw); 2) the areas to the north of the WIPP site that might create additional recharge to the Culebra due to water applied to potash tailings pile; and 3) the limits imposed on the domain size by the available

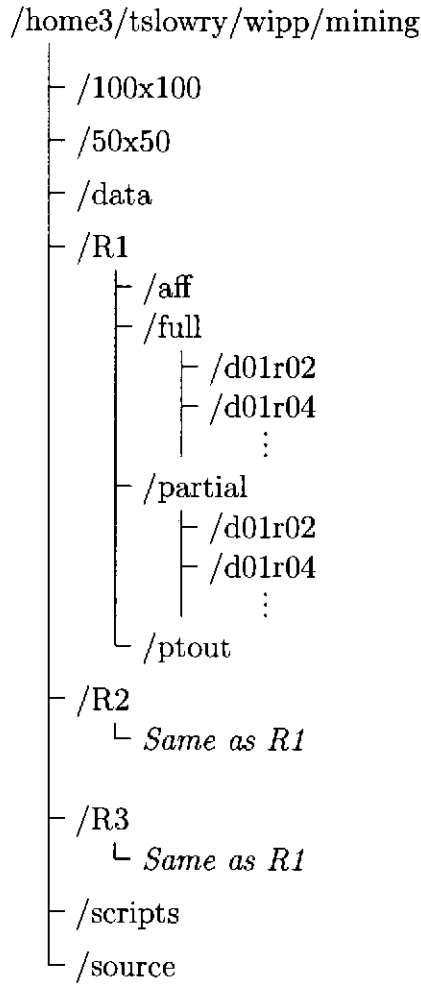


Figure 2: Directory tree of Task 5 files and programs. *Note that the subdirectories d01r02 and d01r04 appearing under the R\*/full and R\*/partial directories represent the first two of 100 subdirectories.*

Table 2: Input and output files used for Task 5. File names in *italics* denote files associated with Tasks 2 and 3 of AP-100.

Directory	File	Description
/mining	Good_runs.txt	List of good T-fields in d##r### format
	mfr*.txt	Mining factors ( $R^* = R1, R2, \text{ or } R3$ )
	Replicate.txt	Replicate number input file
	Full_mining.dat	Full-mining input file
	Part_mining.dat	Partial-mining input file
/100x100	culebra.ibd	IBOUND file
	culebra.ihd	Initial heads
	culebra.top	Culebra top elevations
	culebra.bot	Culebra bottom elevations
	steady.ba6	<b>MF2K</b> basic input file
	steady.bc6	<b>MF2K</b> block-centered input file
	steady.nam	<b>MF2K</b> naming file
	steady.dis	<b>MF2K</b> discretization input file
	steady.oc	<b>MF2K</b> output control file
	steady.lmg	<b>MF2K</b> AMG1R5 solver input file
	dtrkmf.in	<b>DTRKMF</b> file name input
	wippctrl.inp	<b>DTRKMF</b> input file
	/50x50	<i>cNew.ibd</i>
<i>cNew.ihd</i>		Initial heads
<i>cNew.top</i>		Culebra top elevations
<i>cNew.bot</i>		Culebra bottom elevations
<i>steady.ba6</i>		<b>MF2K</b> basic input file
<i>steady.bc6</i>		<b>MF2K</b> block-centered input file
<i>steady.nam</i>		<b>MF2K</b> naming file
<i>steady.dis</i>		<b>MF2K</b> discretization input file
<i>steady.oc</i>		<b>MF2K</b> output control file
<i>steady.lmg</i>		<b>MF2K</b> AMG1R5 solver input file
/R*/[scenario]/ d##r###		CMine.mod
	dtrk.dbg	<b>DTRKMF</b> debug output file
	dtrk.out	<b>DTRKMF</b> output file
	steady100x100.bud	<b>MF2K</b> budget output
	steady100x100.hed	<b>MF2K</b> head output
	steady100x100.lst	<b>MF2K</b> listing file
	<i>steady50x50_ascii.dat</i>	<b>BA.F</b> ASCII budget output
	<i>steady50x50.bud</i>	<b>MF2K</b> flow budget output
	<i>steady50x50.hed</i>	<b>MF2K</b> head output
	<i>steady50x50.lst</i>	<b>MF2K</b> listing file
	<i>TNew.mod</i>	Mining-altered T-field from <b>REFINE.F</b>



computational resources and the desired fine scale discretization of the domain within the groundwater model. The final model domain is rectangular and aligned with the north-south and east-west directions. The coordinates of each corner of the domain are given in Table 1 in UTM (*NAD27*) coordinates. A no-flow boundary corresponding roughly to the center of Nash Draw is shown in Figure 1 [*not shown*] as a purple line extending from the northern to southern boundaries in the western one-third of the model domain. Model cells falling to the west of this boundary are considered to be inactive in the groundwater flow calculations.

The modeling domain consists of 224 cells in the east-west direction (x-direction), and 307 cells in the north-south direction (y-direction). Each cell is of uniform 100 m size on all sides making the modeling domain 22.4 km wide by 30.7 km tall (Figure 3). The discretization of the flow model domain into 100x100 meter cells leads to a total of 68,768 cells: 14,999 (21.8%) inactive cells to the west of the no-flow boundary and 53,769 active cells to the east of the boundary. This number is nearly a factor of 5 larger than the 10,800 (108x100) cells used in the CCA calculations.

The corner coordinates of the modeling domain in UTM NAD 27 are given in Table (3). The CRA-revised and CRA grid differs from the 1996 grid described in Wallace (1996) in that the previous CCA grid was non-uniform and rotated clockwise approximately  $38^\circ$  from the north-south/east-west alignment. In addition, the CCA grid used a non-uniform cell size across the domain with a minimum cell dimension of 100 m square over the LWB area and a maximum cell dimension of 800 m square cells at the corners. The model domains of the CCA grid, CRA grid, and the CRA-revised grid for both the full- and partial-mining scenarios are shown in Figures (4) and (5), respectively.

For the **DTRKMF** particle tracking simulations, a single particle is tracked from the UTM NAD27 coordinate,  $X = 613,597.5$  m,  $Y = 3,581,385.2$  m to the LWB for each T-field and replicate/scenario combination (Ramsey et al., 1996, p. 9). The coordinates of the LWB are shown in Table (4).

## 2.5 Boundary and Initial Conditions

Like the model domain and discretization, the boundary and initial conditions used in the CRA-revised calculations are the same as those used in the

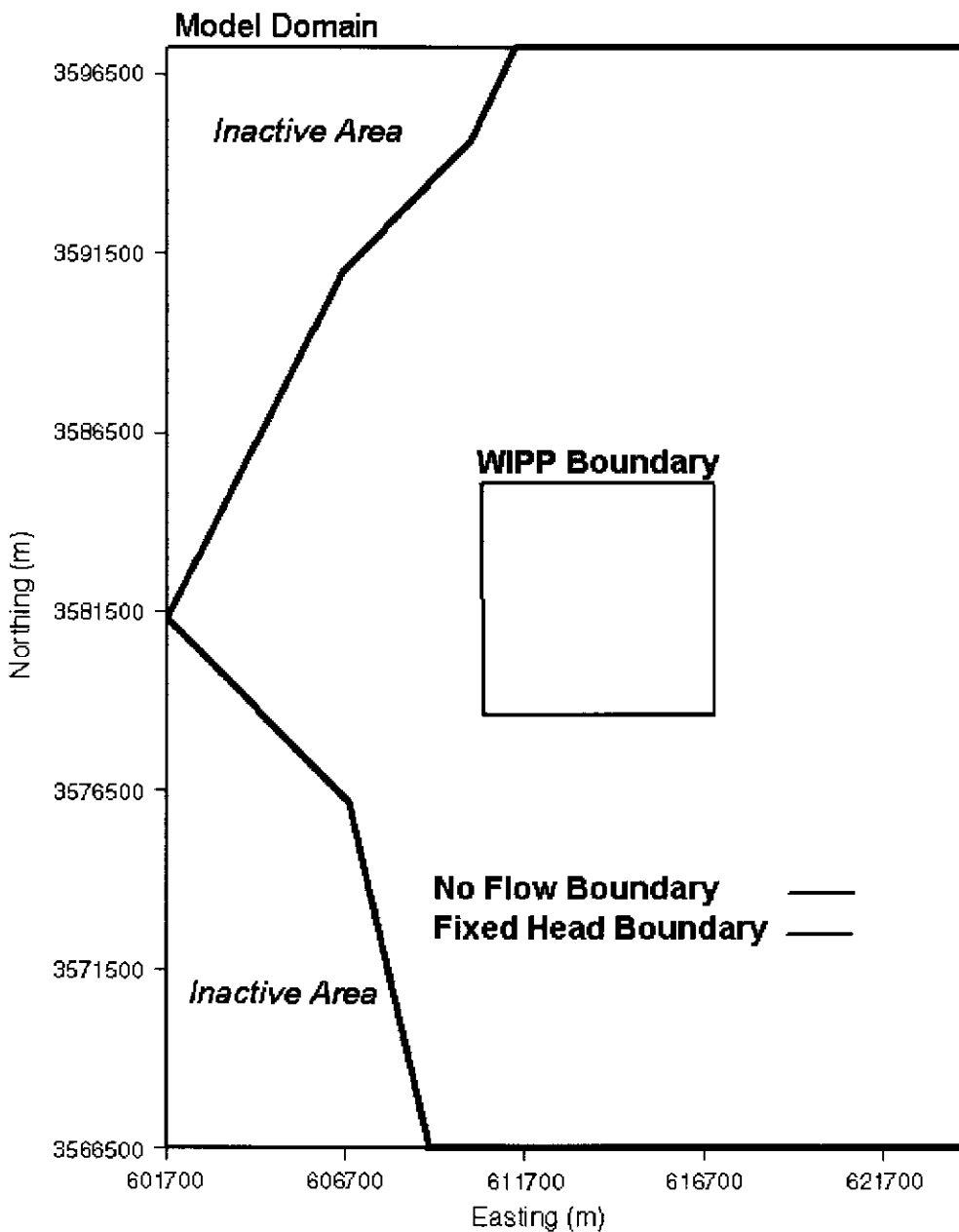


Figure 3: Modeling domain and boundary conditions for the CRA-revised grid configuration. This is the same domain used in the CRA calculations (Lowry, 2003a). The western no-flow boundary coincides with the groundwater divide underneath Nash draw.

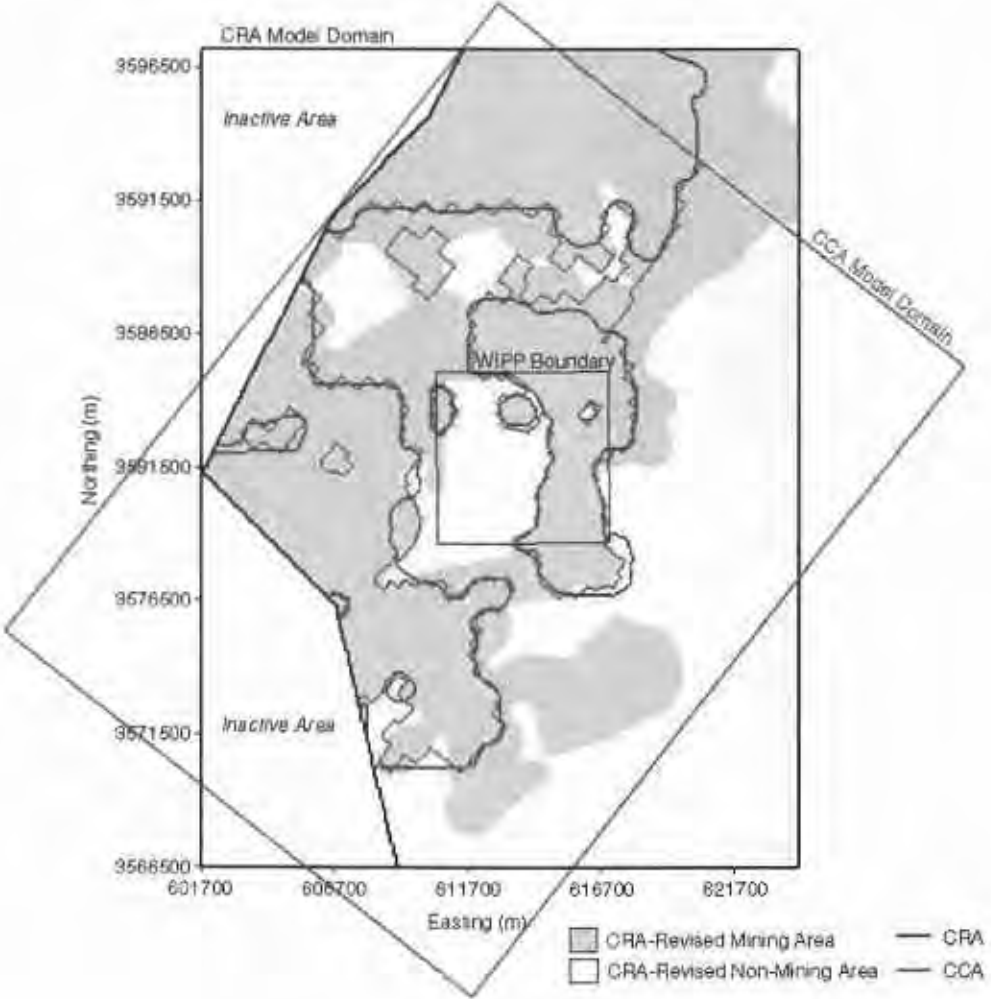


Figure 4: The CRA-revised full mining zones overlaid with the 1996 CCA (red) and CRA delineations (blue).

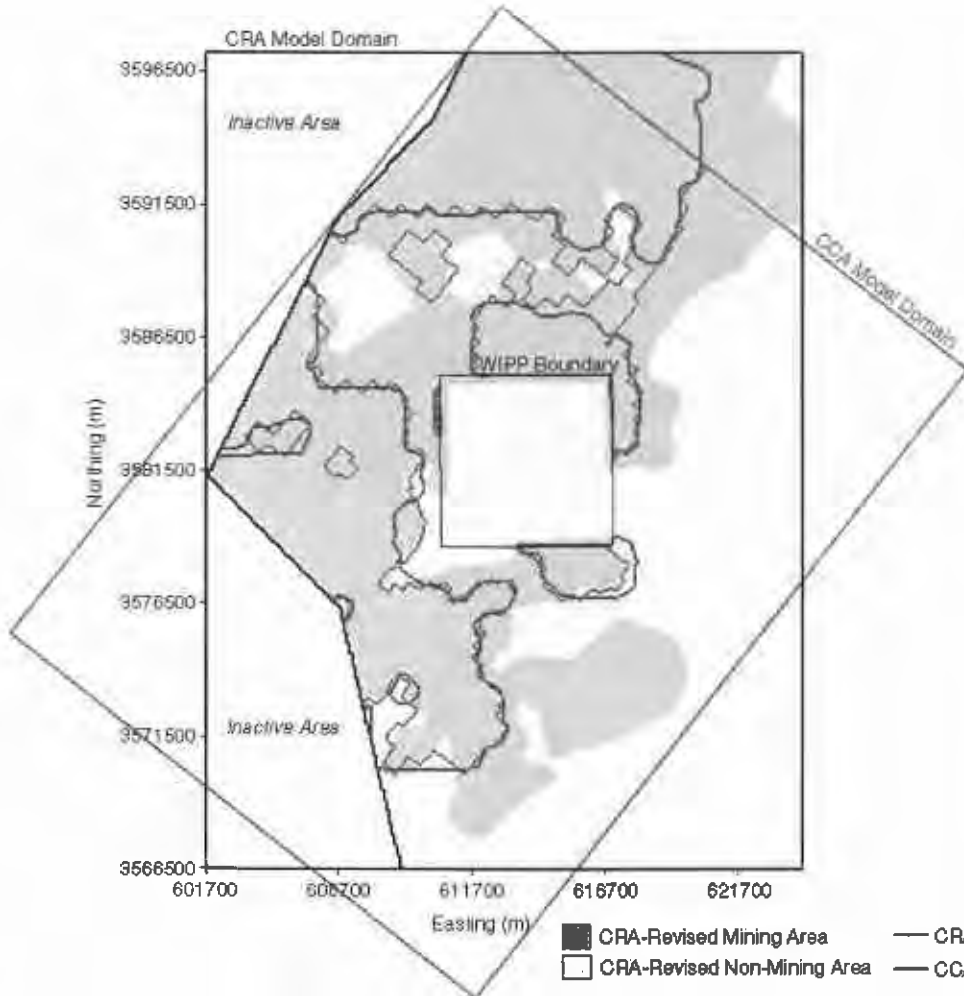


Figure 5: The CRA-revised partial mining zones overlaid with the 1996 CCA (red) and CRA delineations (blue).

Table 3: The coordinates of the corners of the numerical model domain in UTM NAD27 Coordinates.

Domain Corner	X Coordinate (meters)	Y Coordinate (meters)
Northeast	624,100	3,597,200
Northwest	601,700	3,597,200
Southeast	624,100	3,566,500
Southwest	601,700	3,566,500

Table 4: The coordinates of the corners of the WIPP land withdrawal boundary (LWB) in UTM NAD27 Coordinates.

Domain Corner	X Coordinate (meters)	Y Coordinate (meters)
Northeast	616,941	3,585,109
Northwest	610,495	3,585,068
Southeast	617,015	3,578,681
Southwest	610,567	3,578,623

CRA calculations (Lowry, 2003a), and are described fully in McKenna and Hart (2003b). As a summary, field head data from the year 2000 consisting of 37 head measurements across the modeling domain are interpolated to the computational grid using Kriging. A five-parameter Gaussian function is used to de-trend the head data at which point a Gaussian variogram model is used to describe the variability of the head residuals with distance. The variogram model is used to estimate the residuals at each node in the grid. The final step is to add the regional trend back to the estimated residuals using the five-parameter Gaussian function.

The model boundaries along the north, east, and south edges of the domain are considered fixed-head boundaries. The Kriged head values determining the initial heads are assigned to each constant head cell and kept fixed throughout the simulation. Since all simulations for this Task are steady-state, determination of the initial heads are important only in relation to setting the fixed boundary conditions. The irregular western boundary is considered a no-flow boundary and falls roughly along the groundwater divide associated with Nash Draw. Nash Draw is interpreted as a regional groundwater divide, draining the Rustler units to the east and north (and

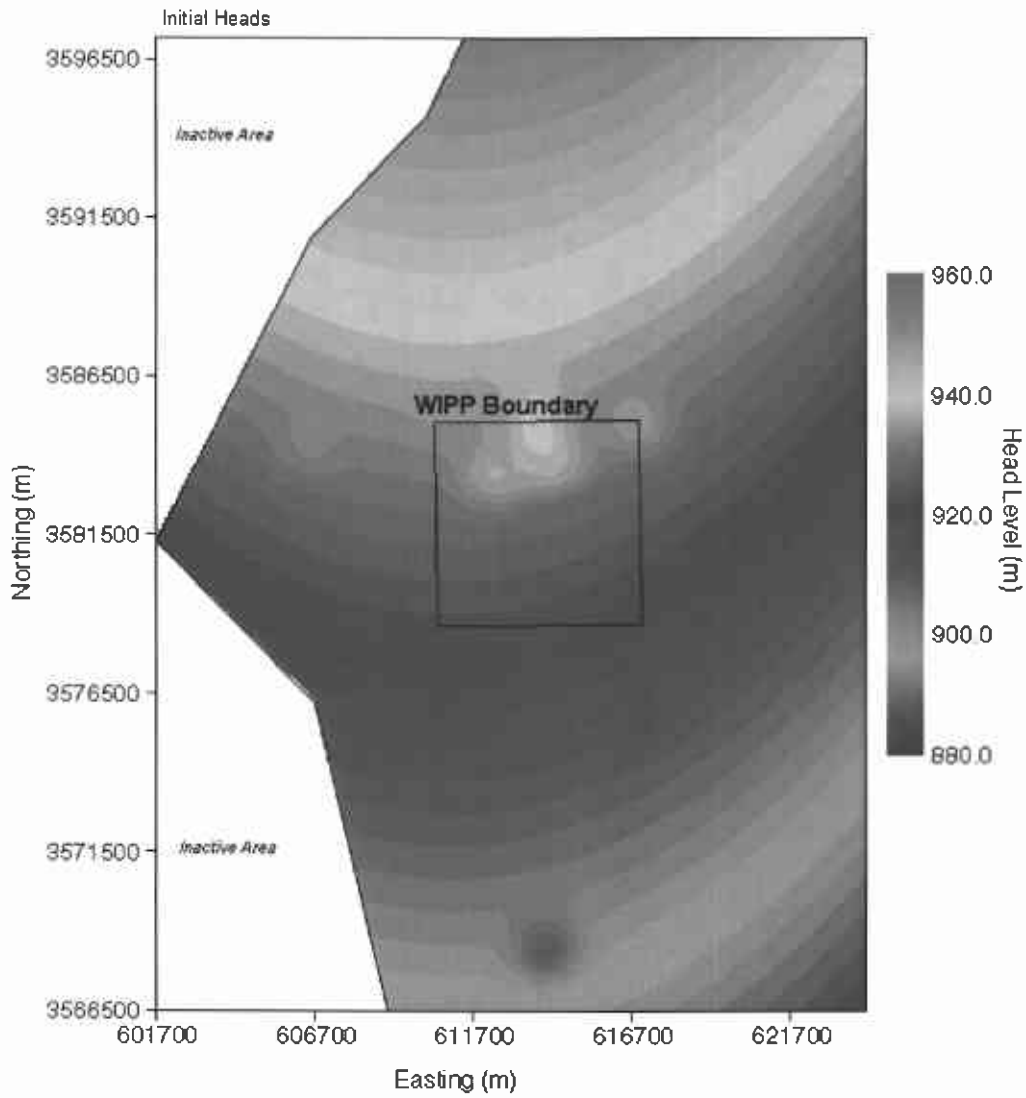


Figure 6: Initial heads across modeling domain.

also by implication via discharge symmetry, to the west). The initial head contours across the active modeling domain are shown in Figure (6).

Since the extent of possible potash mining extends well beyond the modeling domain, the effects of mining on the boundary conditions must be considered. Regional flow rates within the flow model are controlled by the boundary conditions and the hydraulic conductivity distribution. The regional gradient across the domain is approximately 0.0017, which is higher than the 0.001 quoted in Wallace (1996) for the CCA. It should be noted that the regional gradients are difficult to directly compare since the CCA grid is rotated approximately 38° clockwise from the CRA grid. Thus, for the CCA grid, the regional gradient is calculated by taking the difference of the highest constant head in the northern corner of the model and the lowest constant head in the southern end of the model, and dividing by the distance between these two points. For the current grid we average the constant heads along the northern boundary, subtract the average heads along the southern boundary, and then divide by the north-south model domain distance. Using only the cells with the highest and lowest constant heads and dividing by the distance between the two, as was done with the CCA grid, the regional gradient is calculated to be 0.0022, which overestimates the regional behavior. It is assumed that mining impacts would not significantly change this regional gradient and thus the boundary conditions for the mining scenarios are identical to those in Task 4 (McKenna and Hart, 2003b). In addition, the CCA used the same conceptualization (keeping boundary conditions fixed between the mining and non-mining scenarios) and to allow for comparisons between the CCA and the CRA, the same conceptualization is maintained.

## **2.6 Subtask 1: Determination of Potential Mining Areas**

The 2002 version of the original 1993 Bureau of Land Management (BLM) map, "Preliminary Map Showing Distribution of Potash Resources, Carlsbad Mining District, Eddy and Lea Counties, New Mexico" (BLM, 1993), was obtained directly from David Hughes of Washington Regulatory Environmental Services (WRES) as an Autocad DXF file. This map was originally developed for the CCA and is periodically updated as part of the "Delaware

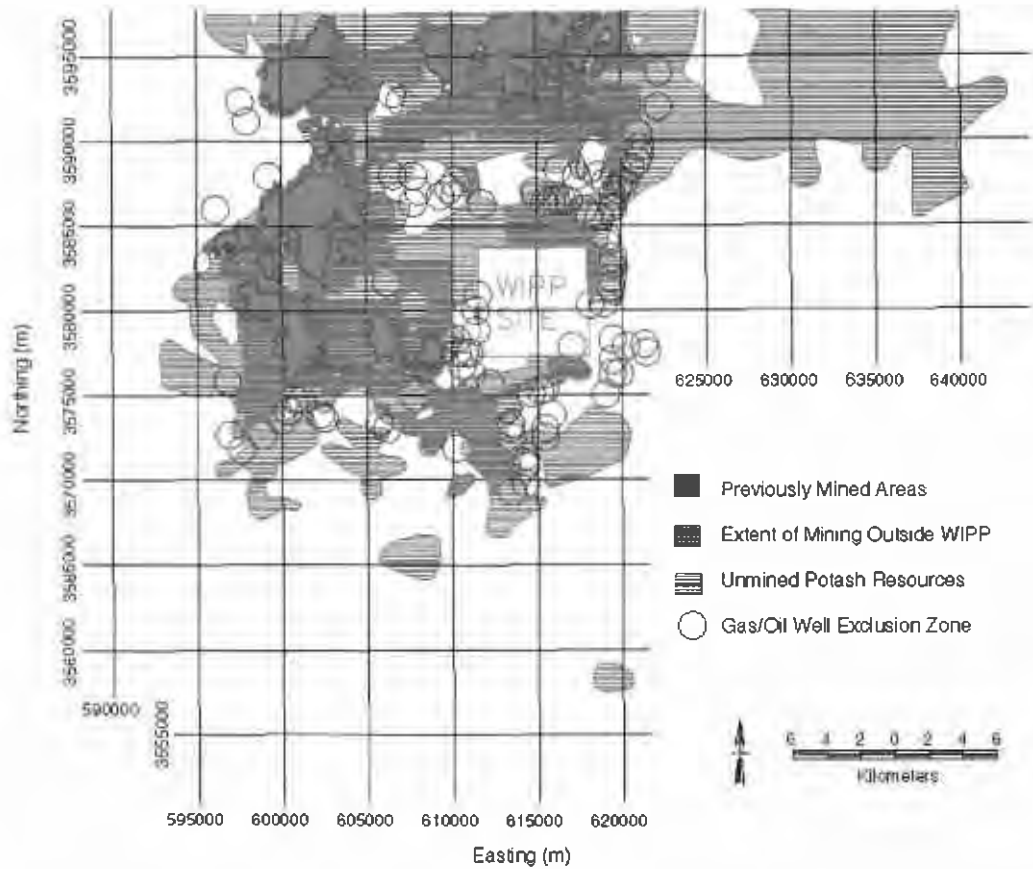


Figure 7: The CRA-revised analysis begins with the un-mined potash resources and possible future mining coverages. The bright blue region designates areas of known mining that were not included in either of the coverages and was manually added to the mining zone area. Coordinates are UTM NAD 27.



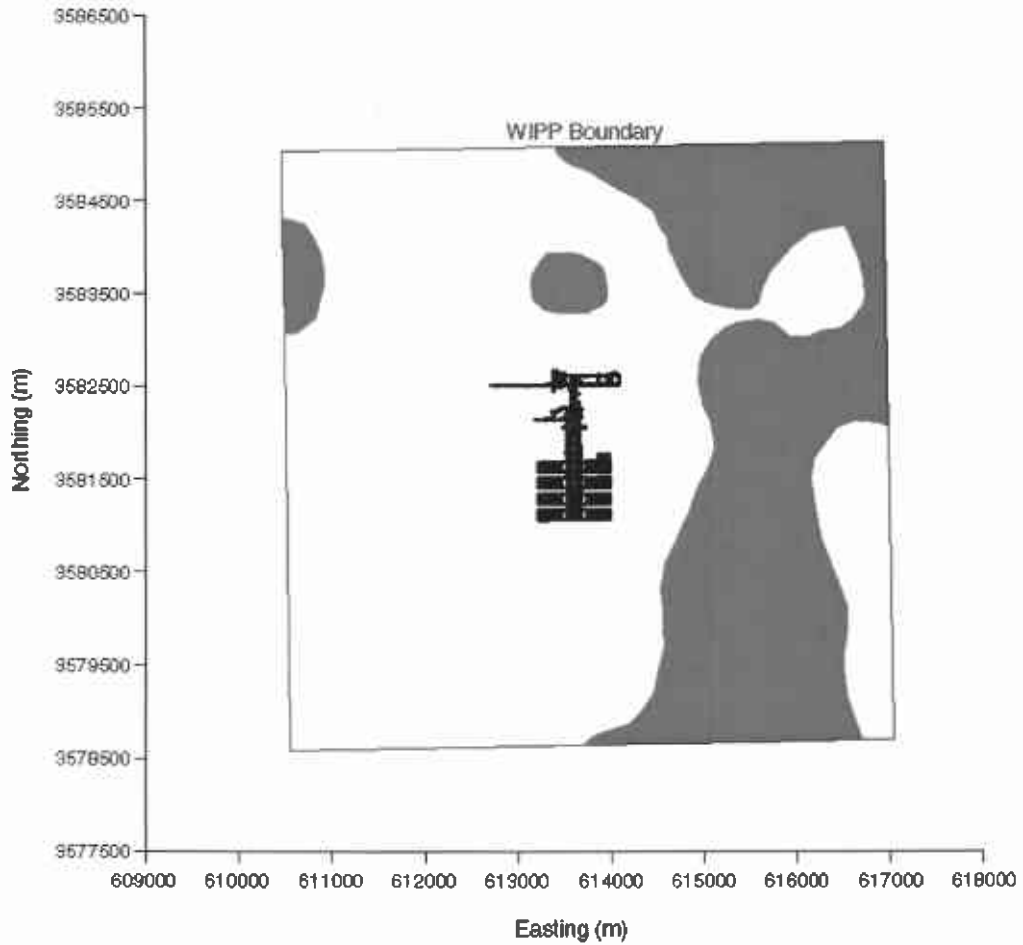


Figure 8: Potential potash distribution within WIPP boundary (red). The repository structure is shown in the center. Coordinates are UTM NAD 27.

Basin Drilling Surveillance Program”, which is performed by WRES.

The coordinates of the DXF file are in State Plane NAD 27, Region 3001 (New Mexico East), and thus required conversion to the UTM NAD 27 (zone 13) system used in this study. The coordinate conversion was done using the Department of Defense groundwater modeling software, **GMS** (GMS, 2003). To address the G-11 comments, two coverages were extracted from the DXF file, ‘Extent of Mining Outside the Controlled Area’ and ‘Unmined Potash Resources’ 7. The first coverage, ‘Extent of Mining Outside the Controlled Area’, delineates areas outside the LWB that have already been mined. This coverage was incomplete in that it did not include a previously mined area in the northern part of the modeling domain (bright blue area of Figure 7). These areas were manually added to the coverage. This combined area was then added to the second coverage, ‘Unmined Potash Resources’ to provide the best estimate of areas with “potential for existing resources to be developed, without substantial deference to whether the leases were currently viable for development” (Cotsworth, 2004). The difference between the CRA-revised delineation and the CRA delineation (Lowry, 2003a) is the CRA eliminates a portion of the area from mining based on the coverage, ‘Mining Boundaries’, which is a set of one-mile diameter circles around each well drilled for oil and gas exploration. These areas are under control of the oil and gas companies and have been deemed as off limits to potash mining. However, as stipulated in comment G-11, the CRA-revised analysis does not include the gas and oil well exclusion zones. In addition, the ‘unmined potash resources’ coverage was included here to gain all areas of possible future potash mining, regardless of current economic viability. The addition of these zones significantly increases the potential potash mining area (Figures 4 and 5) over that of the CRA (Lowry, 2003a).

Since the potash mining area is located in the Salado Formation, below the Culebra, the areas disturbed by mining activities in the Culebra are larger than what is shown on the the BLM map due to subsidence-induced angle-of-draw effects. The rationale for determining the extent of these effects is described in Wallace (1996) with the final conclusion stating that an additional 253 m wide ‘collar’ was to be added to the mining-impacted areas. This is considered a conservative estimation of the angle-of-draw effects. To accommodate the angle of draw, the mining zone boundaries, as overlaid on the current model grid, were moved outward 3 cells in the x and y directions (300 m), and 2 cells in the diagonal direction (283 m). The CRA-revised modeling domain and mining zones for the full-mining case are shown in

comparison to the 1996 CCA and the CRA (Lowry, 2003a) delineations in Figure (4). A closeup of the WIPP site and the associated mining zones is shown in Figure (8). The partial-mining case is shown in Figure (5).

The output of this delineation is a file that contains one value for each cell in the grid. A value of 0 is an inactive cell, a value of 1 means the cell lies within a potential mining zone, and a value of 2 means it lies outside a potential mining zone. One file for each scenario, full-mining and partial-mining, is generated, and used as input to the data conversion programs, **FM.F** and **PM.F** respectively.

## **2.7 Subtask 2: Use of Mining Zones in Forward Simulations**

The calibration process in McKenna and Hart (2003b) produces a transmissivity field that minimizes the error between the steady-state and transient head distributions and the calculated distributions using the calibrated field. Since the calibration process does not produce a unique solution, i.e. given a different set of starting transmissivities a different final set of transmissivities may be reached, multiple T-fields are produced and 100 are selected based on the criteria set forth in Beauheim (2003). To simulate the effects of mining, each selected T-field is multiplied by its own unique mining scaling factor in areas of potential mining, and **MF2K** is run to produce the mining-affected head distribution and the cell-by-cell flow budget files. The cell-by-cell flow budget file is used for input to Subtask 3. To assure repeatability, three different sets of mining factors are used, each set forming a replicate. Thus, for each mining scenario (full and partial), 3 sets of 100 mining-altered T-fields are produced. The same mining factors used for the CRA are use in the CRA-revised analysis. The random mining factors are reproduced in Appendix (A).

## **2.8 Subtask 3: Particle Tracking using DTRKMF**

A single particle is tracked from the UTM NAD27 coordinate  $X = 613,597.5$  m,  $Y = 3,581,385.2$  m to the LWB for each T-field and replicate/scenario combination, using the code **DTRKMF**. Two outputs are generated from the suite of particle tracks. First are plots showing the individual tracks for all 100 T-fields in each scenario for each replicate (6 plots total). This allows for visual comparison of the prevailing flow directions for the full- and partial-mining scenarios and the qualitative comparison of the variability of the tracking direction. Secondly, cumulative distribution func-

tions (CDF's) are constructed for each replicate and scenario. The CDF's describe the probability that a particle will cross the LWB in a given amount of time. The six plots and the CDF's are presented below in the results section.

### 3 Modeling Assumptions

Besides assumptions inherent in all modeling exercises (e.g. physical processes can be adequately parameterized and estimated on a numerical grid) there are several assumptions that are specific and important to the CRA-revised analysis. Those assumptions are as follows:

1. It is assumed that the boundary conditions along the model domain boundary are known and are not dependent on mining. The reasoning for this assumption is described in Section 2.5.
2. It is assumed that the flow-field over the duration of the particle tracking and transport times can be adequately represented by steady-state conditions. This is related to the first assumption in that the boundary conditions are also assumed to remain constant over time. This assumption is necessary since data do not exist that can predict the transient conditions at the site over the time frames involved (>100,000 years).
3. It is assumed that the mining effects can be adequately represented with a single mining factor that increases the transmissivity uniformly across the potential mining zones within the Culebra. This is directed by EPA regulation 40CFR Part 194, p. 5229 and is assumed adequate for this Task. The regulation is included as an appendix in Wallace (1996).
4. Mining will occur in the previously omitted 1 mile radius exclusion zones around existing oil and gas wells as well as all regions with identified potash resources.

Other assumptions related to this analysis can be found in McKenna and Hart (2003b).

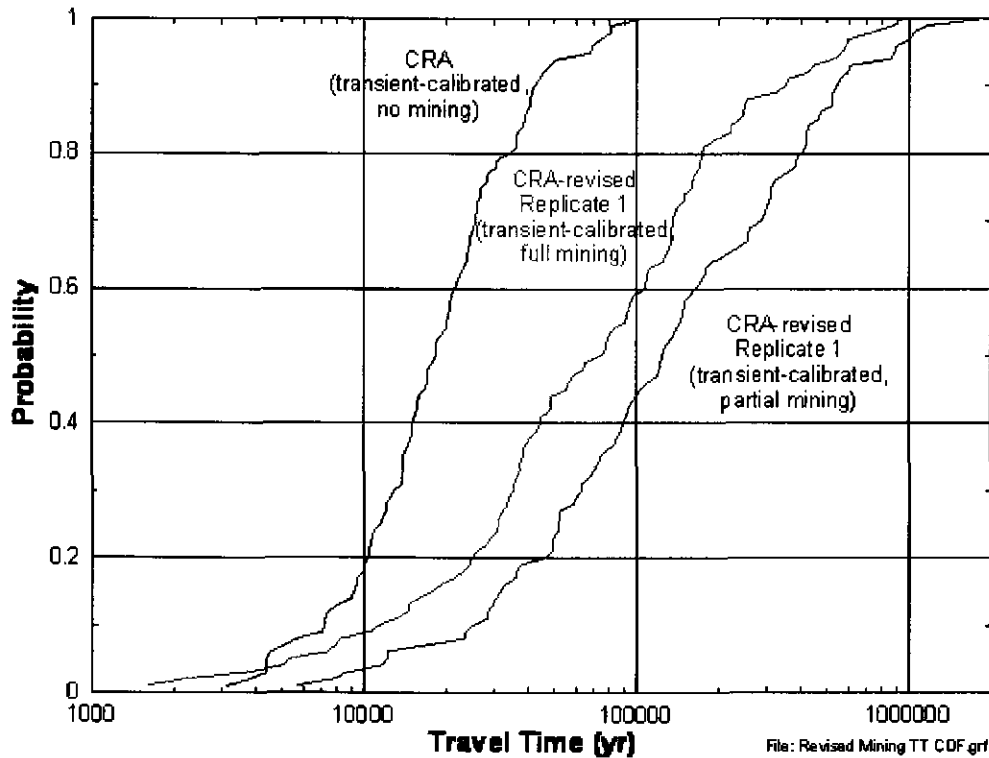


Figure 9: Cumulative distribution function plot of the full-, partial-, and non-mining scenarios for the CRA-revised calculations.

## 4 Results

### 4.1 Particle Travel Times

Compared to the non-mining scenario, the travel times for both mining scenarios are longer; the median travel times across all 3 replicates for the full- and partial-mining scenarios are approximately 4.14 and 7.06 times greater than for the non-mining scenario, respectively. This is greater than either the CCA or CRA calculations (discussed more below). A plot of the cumulative distribution functions (CDFs) for the full-, partial-, and non-mining scenario's is shown in Figure (9).

Given the increase in transmissivity due to mining, the increase in travel time may seem counter-intuitive. However, upon examination of the head

Table 5: Travel time statistics (median, maximum, & minimum) in years for the full and partial mining scenarios as compared to the CRA and non-mining scenarios.

Replicate	Stat.	CRA-Revised		CRA		Non-Mining
		Full	Partial	Full	Partial	
R1	Med.	75,410	125,712	63,370	47,745	NA
	Max.	941,529	1,882,522	504,174	494,981	
	Min.	1,615	5,645	723	4,684	
R2	Med.	73,327	127,265	73,169	47,651	
	Max.	2,196,690	2,499,469	3,387,185	531,136	
	Min.	2,178	5,573	611	4,654	
R3	Med.	76,097	135,686	63,430	51,622	
	Max.	944,251	5,195,535	1,610,979	506,437	
	Min.	1,550	5,635	615	4,603	
Global	Med.	75,774	129,202	66,048	48,290	18,289
	Max.	2,196,690	5,195,535	3,387,185	531,136	101,205
	Min.	1,550	5,573	611	4,603	3,111

contours and flow patterns of the mining cases, the high transmissivity areas corresponding to the mining zones create preferential pathways through the system. Figure (10) shows the normalized velocity in each cell for the T-field/replicate averaged case for the full-mining scenario. The normalized velocity is the velocity magnitude in each cell divided by the maximum velocity magnitude across the domain. ‘T-field/replicate averaged’ means the transmissivity value for each cell is the average of the transmissivities across all T-field/replicate combinations for the full-mining scenario (300 T-fields in total). Not surprisingly, it is clear that the areas of high velocities correspond with the mining zones. The higher velocities and corresponding higher flow rates through the mining zone areas translate to slower velocities in the non-mining zone areas. Since the starting point for the particle tracking is in a non-mining area, travel times are increased as compared to the non-mining scenario. A comparison of the median, maximum, and minimum values for the full-, partial-, and non-mining scenario travel times is presented in Table (5).

A comparison to the CCA and CRA (Lowry, 2003a) results provides

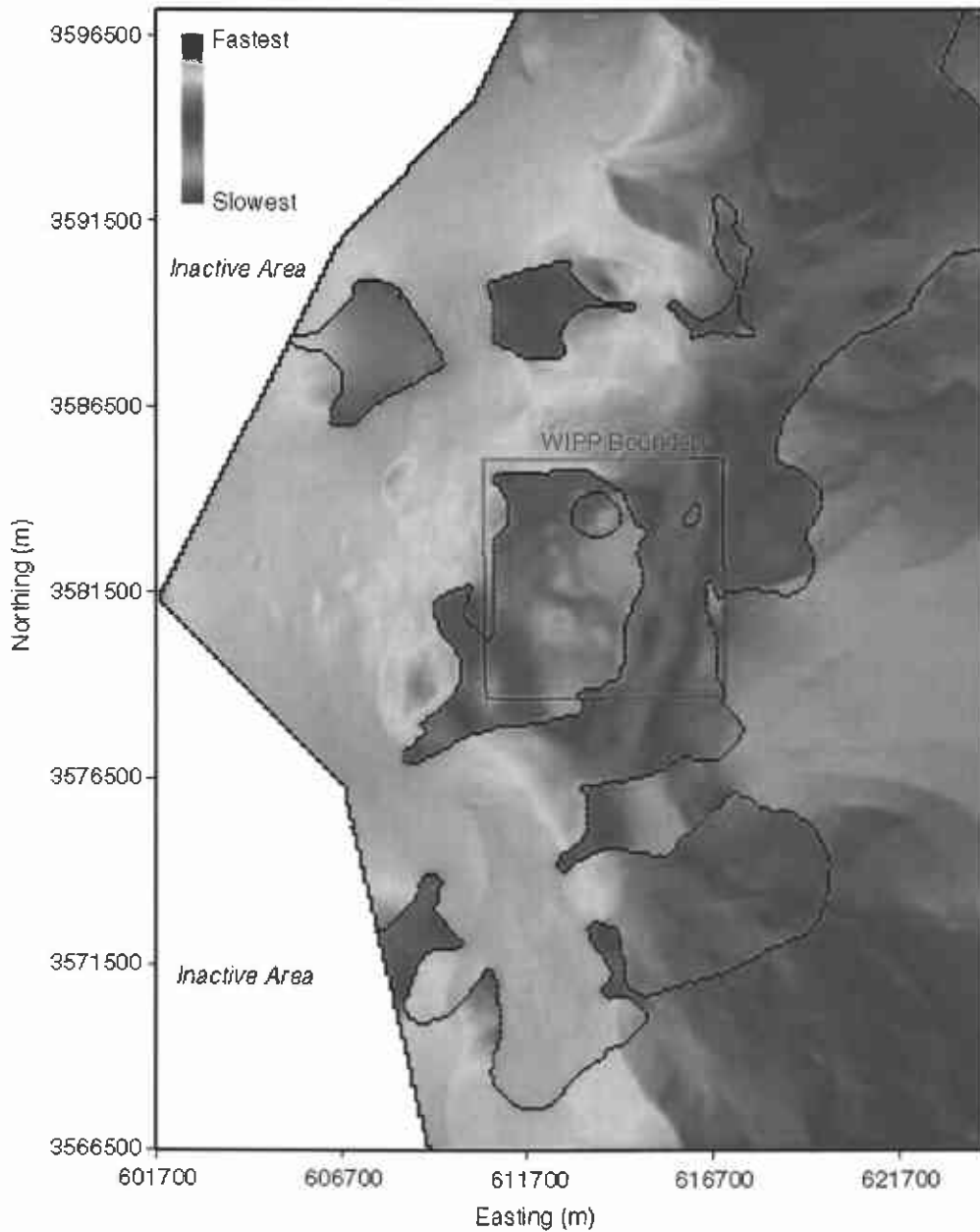


Figure 10: Normalized pore velocities for the full-mining case. Red indicates zones of highest velocity. The black lines show the full-mining zones and the red box is the WIPP LWB. The T-field used to produce the velocity profile is averaged across all T-field/replicate combinations for the full-mining scenario (300 T-fields in total).

perspective on the impact of the changes between the CCA, the CRA, and the CRA-revised analysis. Figures (11) and (12) show the CDF's for the CRA-revised full- and partial-mining scenarios, respectively, for all three replicates as compared to the CCA and CRA results. The CRA results are also listed with the current results in Table 5. The median travel times for the CRA-revised analysis is approximately 1.15 and 2.68 times longer for the full- and partial-mining scenarios, respectively, than for the CRA scenarios and 2.52 and 9.36 times longer than for the CCA scenarios. This is mainly due to the difference in how the base T-fields are generated and the amount of total area that is designated as mining zone. The CCA fields use a categorical simulation technique to capture both high transmissivity (T) and low T regions. In contrast, the CRA (McKenna and Hart, 2003b) and CRA-revised T-fields incorporate more geological understanding, with regions to the west categorized as high T, regions to the east categorized as low T, and the area in between given high or low T on a stochastic basis. This results in significant differences in T for the CRA and CRA-revised domains in the southern part of the WIPP site as compared to the CCA. The CCA fields tend towards lower and more uniformly distributed T's in the southwestern portion of the WIPP site with a high T channel down the southeastern part of the site that leads to shorter travel times than the CRA. The fields used in the CRA and the CRA-revised show higher T's in the southwestern part of the WIPP site and tend not to have the high T channel in the southeast, causing travel times to increase. Additionally, as the total mining zone area increases as between the CRA and the CRA-revised, more flow is diverted around the WIPP site, causing slower velocities in the non-mining zones and longer travel times.

## 4.2 Travel Direction

For the CRA-revised full mining scenario, travel directions are significantly different than the CRA (Lowry, 2003a). A wider mining zone to the west of the WIPP site in the CRA-revised delineation decreases the total flow through the mining area on the east boundary of the WIPP site, lowering the relative heads to the east and causing particles to move eastward towards the boundary between the mining and non-mining zone. Most particles tend to seek out this boundary and then move southward along that boundary. This is in contrast to the partial-mining scenario where the tracking direction for the CRA-revised is similar to the CRA as well as to the non-mining scenario.



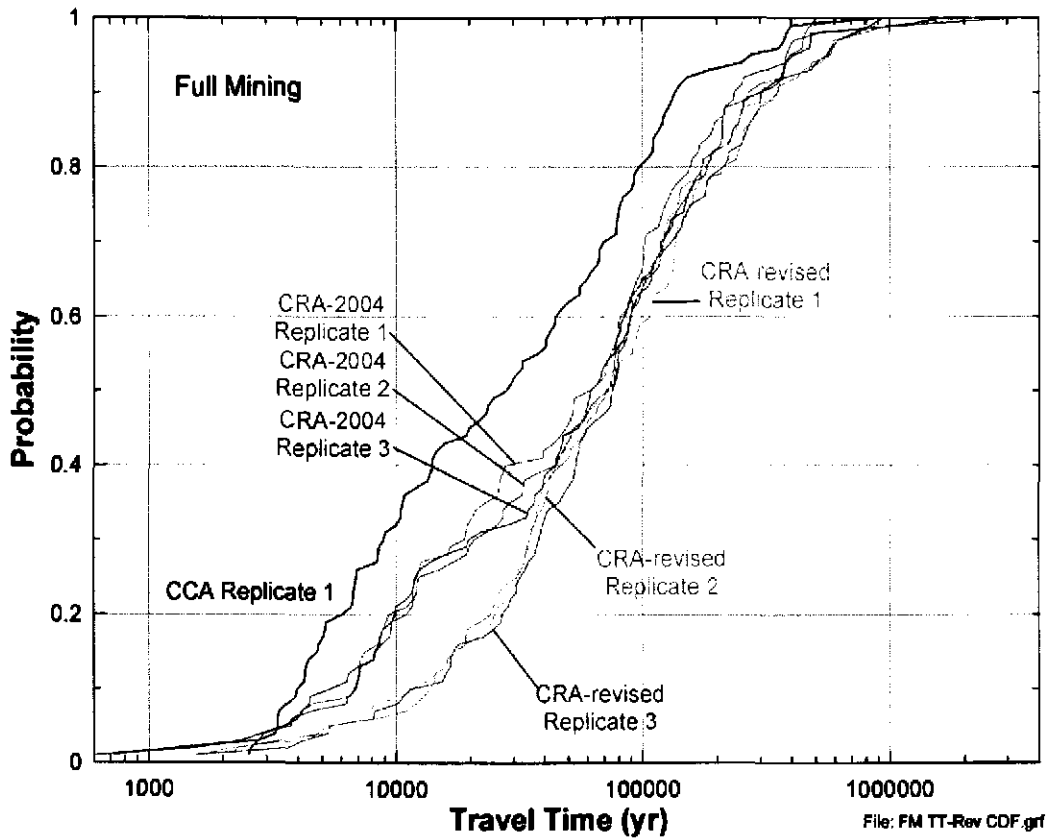


Figure 11: Cumulative distribution function plot for the CRA-revised calculations of the 3 full-mining scenario replicates as compared to the CRA and CCA full-mining scenarios. An increase in travel time can be seen over the previous calculations.

The particle track directions for the full- and partial-mining scenarios are illustrated in Figures (13) to (18). Like the CRA, there is a strong similarity within each replicate for each scenario. With slight variations, individual tracks can be recognized from one replicate to the next. This indicates that particle track directions are determined more by the spatial variation of the calibrated T-field than by the random mining factors, although the random mining factors have a greater effect for the CRA-revised than in the CRA calculations (Lowry, 2003a).

Correlation analysis for the CRA-revised calculations show correlations

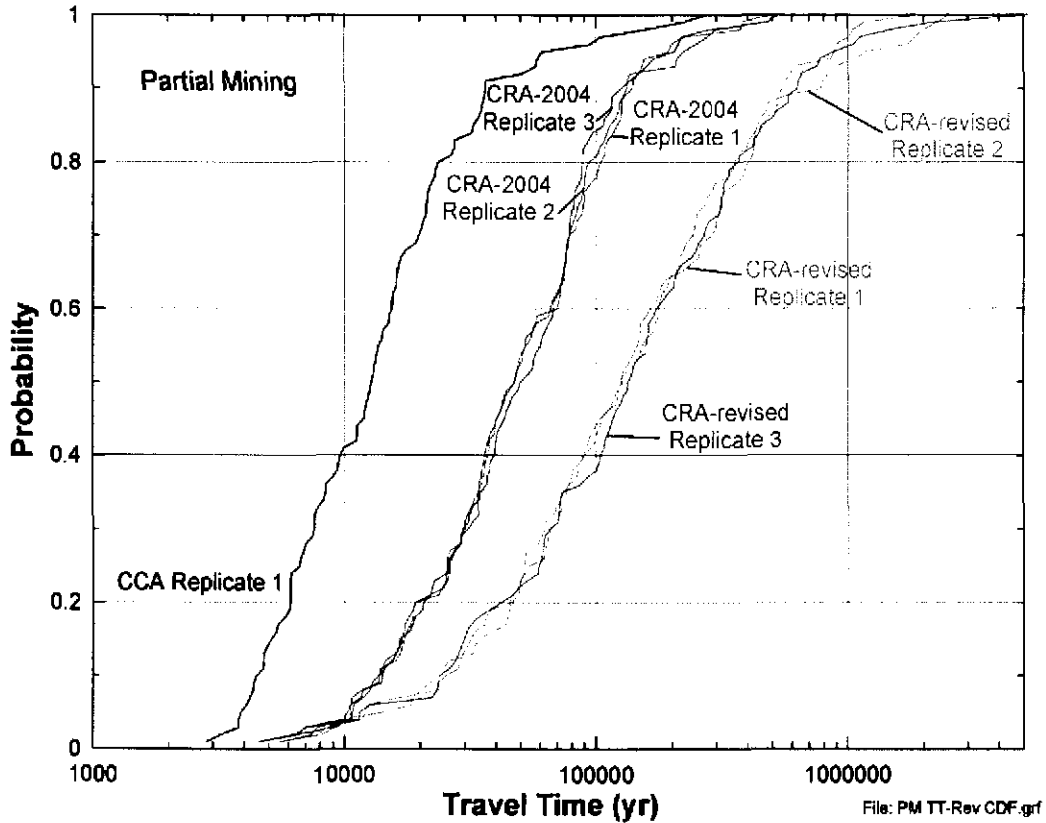


Figure 12: Cumulative distribution function plot for the CRA-revised calculations of the 3 partial-mining scenario replicates as compared to the CRA and CCA partial-mining scenarios. An increase in travel time can be seen over the previous calculations.

between travel time and the random mining factor for the full and partial-mining scenarios as 0.32 and 0.30, respectively. This compares to correlation factors of 0.09 (full mining) and 0.15 (partial mining) for the CRA (Lowry, 2003a). Figure (19) shows the  $Log_{10}$  travel times versus the random mining factor for the full- and partial-mining scenarios across all replicates for the CRA-revised. Like the particle travel directions, this increase in correlation between the random mining factor and the travel time can be explained by the increase in area of the mining zones. The flow fields in the CRA-revised analysis are highly influenced by the large area to the west of the WIPP site

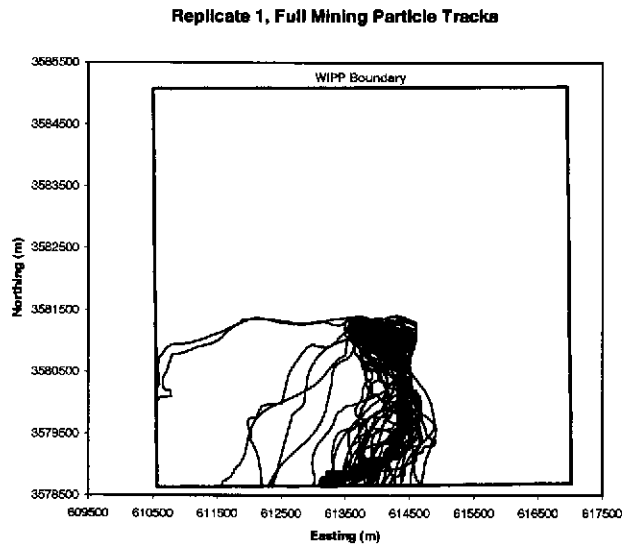


Figure 13: Particle tracks of the CRA-revised calculations for replicate 1 for the full-mining scenario.

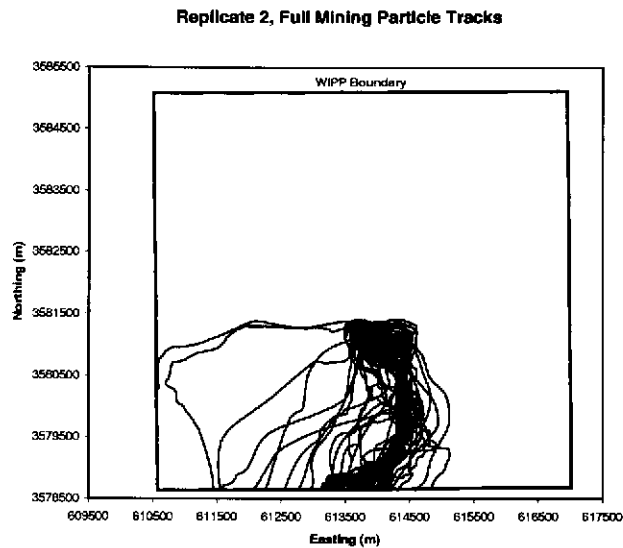


Figure 14: Particle tracks of the CRA-revised calculations for replicate 2 for the full-mining scenario.

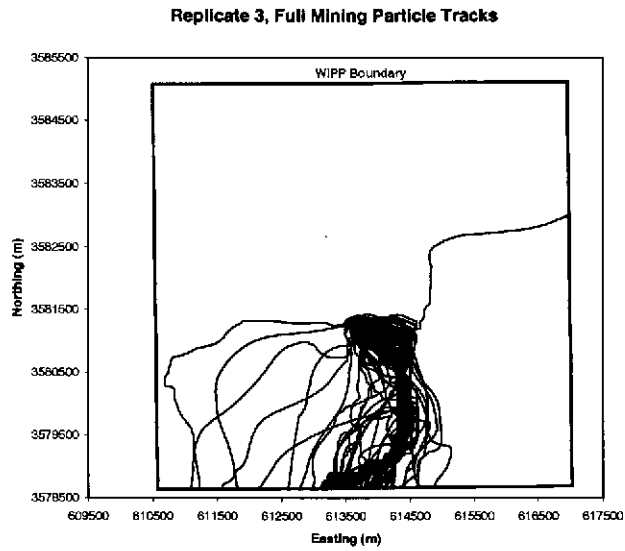


Figure 15: Particle tracks of the CRA-revised calculations for replicate 3 for the full-mining scenario.

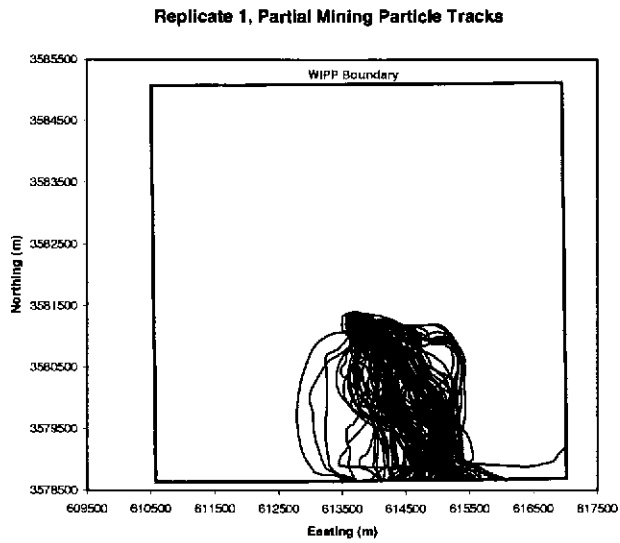


Figure 16: Particle tracks of the CRA-revised calculations for replicate 1 for the partial-mining scenario.

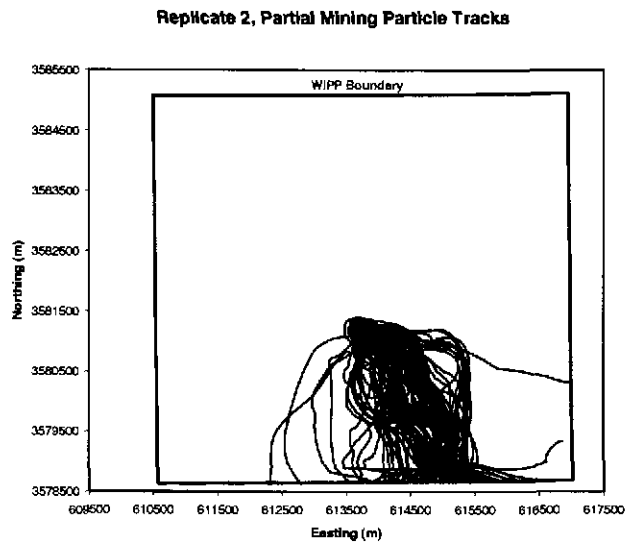


Figure 17: Particle tracks of the CRA-revised calculations for replicate 2 for the partial-mining scenario.

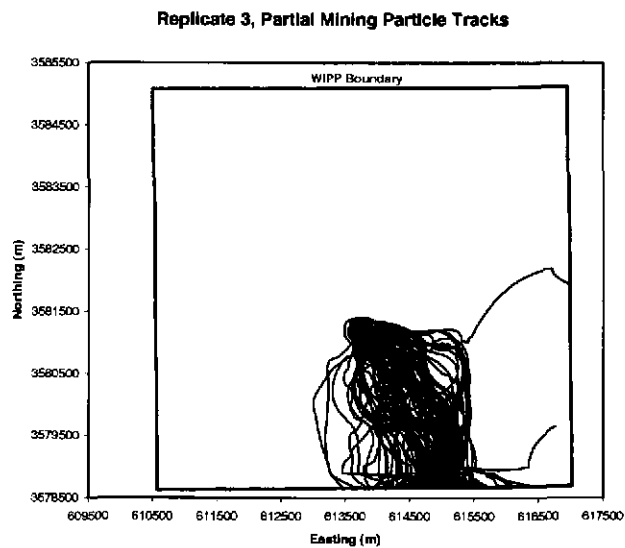


Figure 18: Particle tracks of the CRA-revised calculations for replicate 3 for the partial-mining scenario.

that is deemed as mining zone. This can be seen in the velocity plot in Figure (10). Since this area is much larger in the CRA-revised analysis than it was in the CRA, a change in transmissivity to this area has a greater regional impact. An increase in transmissivity in the mining zone means higher flow rates through those areas, and correspondingly lower flow rates through the non-mining zone areas. The high scatter shown in Figure (19) indicates that the transmissivity spatial distribution plays a significant role in determining the travel time. The standard deviation of the  $\text{Log}_{10}$  travel time due only to differences in the T-field is 0.5 for both the full- and partial-mining scenarios. With the assumption that the variability around the trendline of Figure (19) is normally distributed, then most values will fall within  $\pm 3$  standard deviations of the trendline. This means that the T-field spatial distribution accounts for the majority of the 3 orders of magnitude range of travel times.

### 4.3 Extreme Values

Examination of the extreme travel time values is useful for quantifying the range of outcomes caused by uncertainty incorporated into the models. For the full-mining scenario, T-field d22r06-R2 (R2 = replicate 2) had the longest travel time of 2,196,690 years. In contrast, T-field d03r03-R3 had the shortest travel time of 1550 years. The median travel time (75,774 years) is best represented by T-field d12r08-R3 (the CRA calculations give maximum, minimum, and median travel times for the full mining scenario of 3,387,185, 611, and 66,215 years, respectively). Figures 20 to 22 show the head contours for each of these cases along with the corresponding particle track. In all cases, the particle track tends to migrate towards and follow the mining boundary to the east of the starting location. What distinguishes the plots is the head distribution across the regions. For the slow case (Figure 20) the head contours to the west of the repository are spread far apart, indicating high transmissivities in the mining zone areas and correspondingly lower velocities in the non-mining zone areas. In contrast, the fastest case (Figure 21) shows a large gradient drop across the same region, resulting in relatively higher velocities in the non-mining areas. The median case (Figure 22) is visually similar to the slowest case.

The partial-mining cases have similar characteristics to that of the full-mining cases (Figures 23 to 25), with areas of mining showing widely spaced head contours. The notable exception is that for the maximum travel time case (Figure 23), the particle travel direction is to the east. The maximum

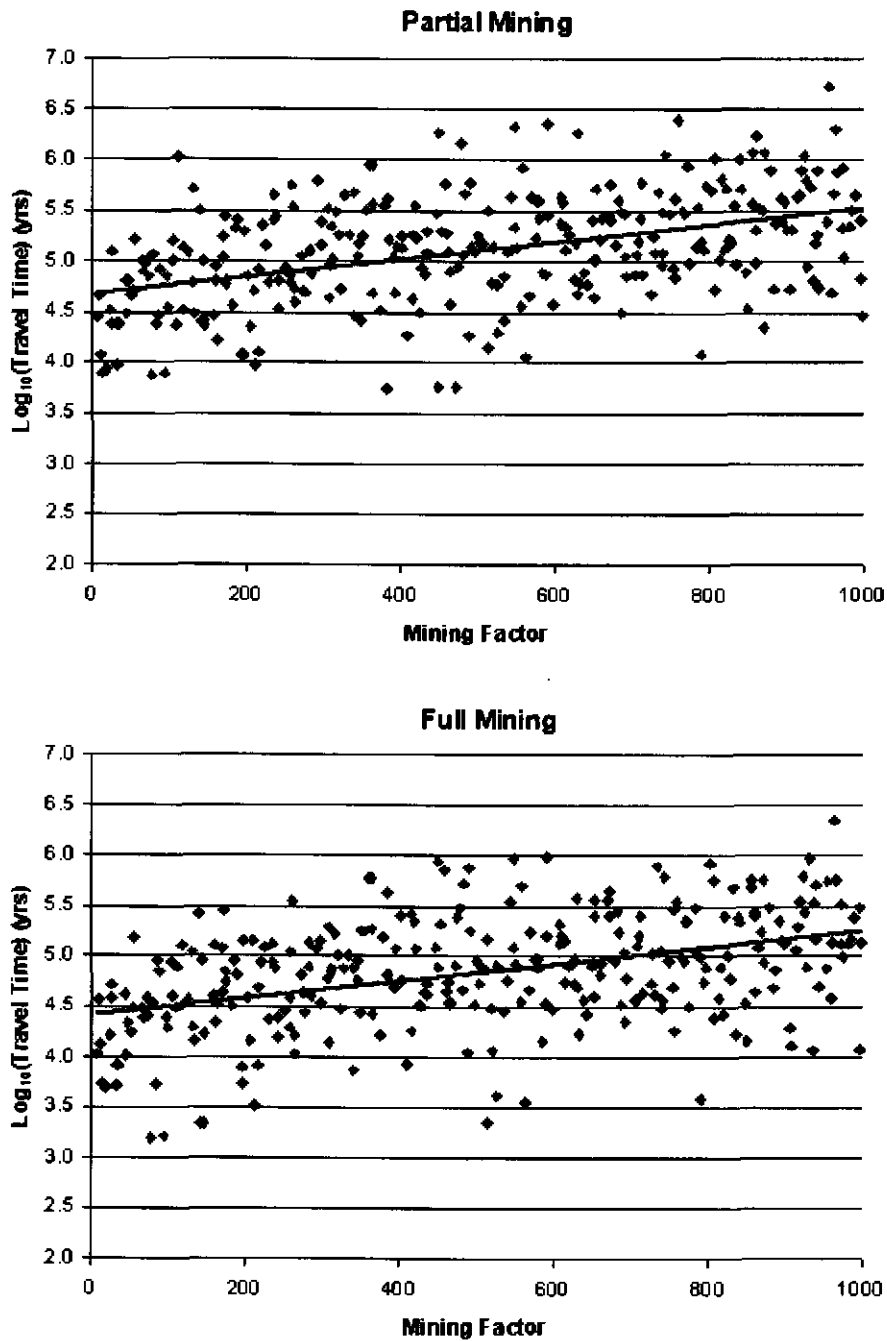


Figure 19: Correlation between the random mining factor and Log-travel time.

(5,195,535 years), minimum (5,573 years), and median (129,202 years) travel times are represented by T-fields d03r01-R3, d09r06-R2, and d13r07-R2, respectively (Figures 24 to 25).

## 5 Summary

This report addresses comments made by the EPA in response to modeling efforts pertaining to the effects of potash mining on flow and advective transport in the Culebra aquifer. Specifically, it is the response to comment G-11 of the EPA CRA Completeness Report, "Letter to R.P. Detwiler, Acting Manager, Carlsbad Field Office, U.S. Department of Energy from E. Cotsworth, Director, Office of Radiation and Indoor Air, U.S. Environmental Protection Agency, September 2, 2004" (Cotsworth, 2004). The intent of comment G-11 is to reform the mining areas to include all areas of unmined potash resources as well as the 1 mile radius exclusion zones around oil and gas wells. This new delineation is known as the CRA-revised analysis. Mining calculations done as part of the CRA (Lowry, 2003a) did not include the 1 mile radius exclusion zones as part of the potential mining areas and also used a more stringent criteria to determine areas of potential potash mining. This analysis re-calculates the mining scenarios addressed in the CRA (Lowry, 2003a) using new mining zone delineations.

Two categories of mining-impacted transmissivity fields are modeled: one with mining outside the land withdrawal boundary (LWB) only and the other with regions both inside and outside the LWB mined (partial and full-mining scenario's, respectively). Flow modeling is performed starting with 100 stochastically calibrated T-fields from McKenna and Hart (2003b). Each T-field is modified to reflect the effects of mining by multiplying the transmissivity value in cells that lie within designated mining zones by a random factor between 1 and 1000. A forward steady-state flow simulation is run for each new T-field under each mining scenario (full and partial) across three replicates of mining factors, resulting in 600 simulations (there are 100 calibrated T-fields from Task 1 of AP-100). Particle tracking is performed on the modified flow fields to determine the flow path and groundwater travel time from a point above the center of the WIPP disposal panels to the LWB. Cumulative probability distribution functions (CDF) are produced for each mining scenario and compared to the undisturbed scenario generated from Task 4 of AP-088, as well as to the full- and partial-mining scenarios from



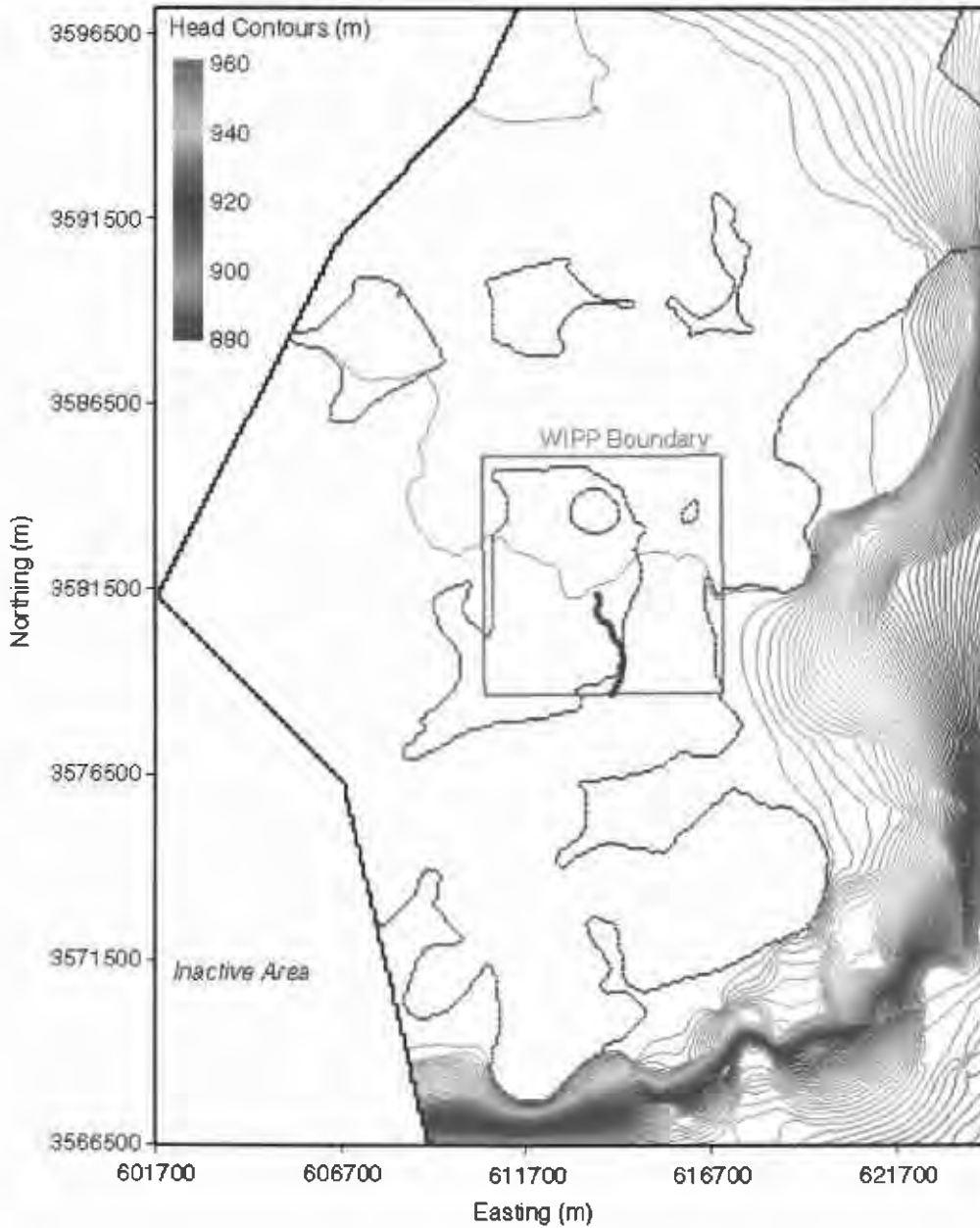


Figure 20: Head contours and particle track for the maximum travel time T-field (d22r06-R2) for the full-mining case. The WIPP boundary is the red box in the center of the figure and the particle track is the blue track originating from the approximate center of the WIPP.

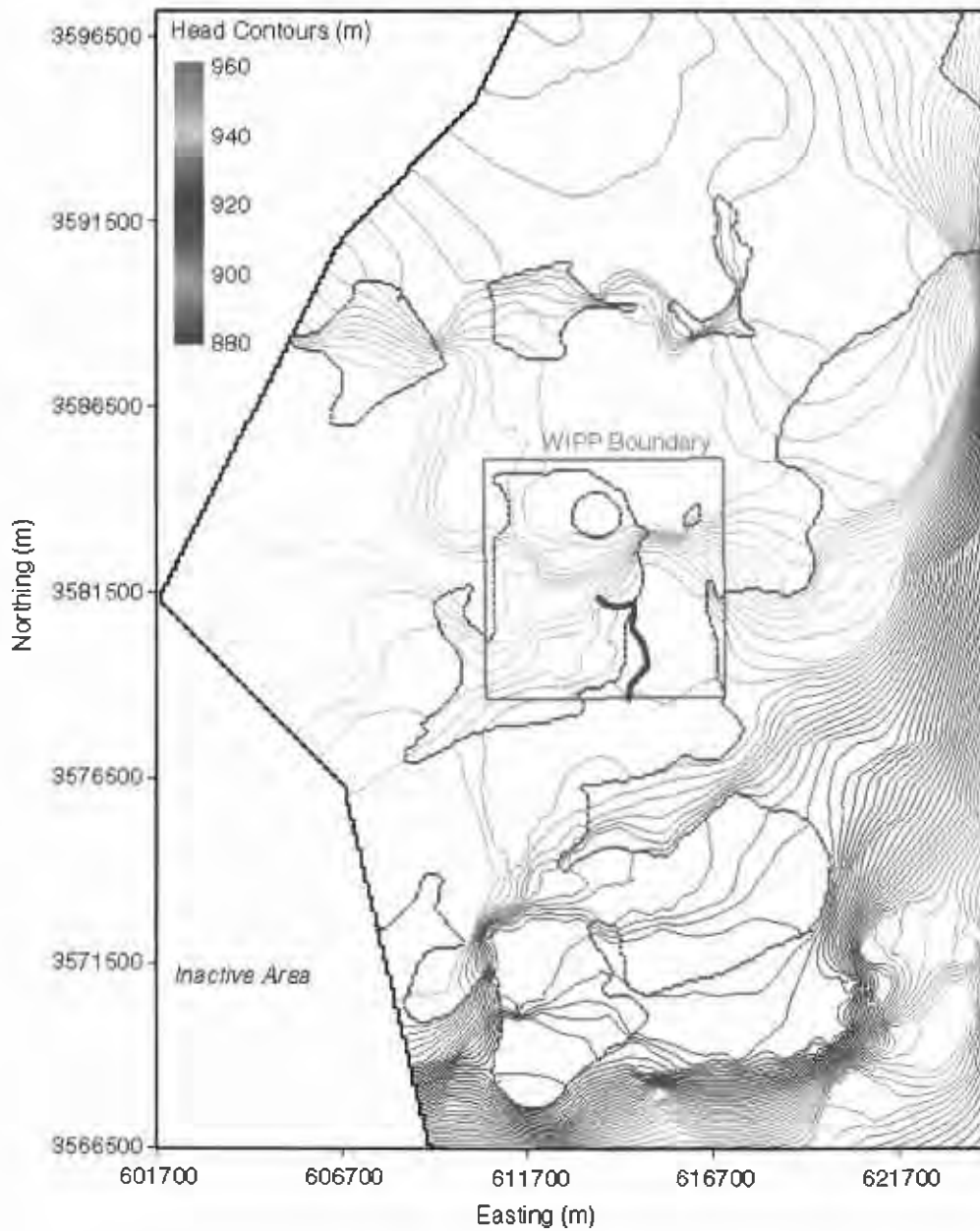


Figure 21: Head contours and particle track for the minimum travel time T-field (d03r03-R3) for the full-mining case. The WIPP boundary is the red box in the center of the figure and the particle track is the blue track originating from the approximate center of the WIPP.

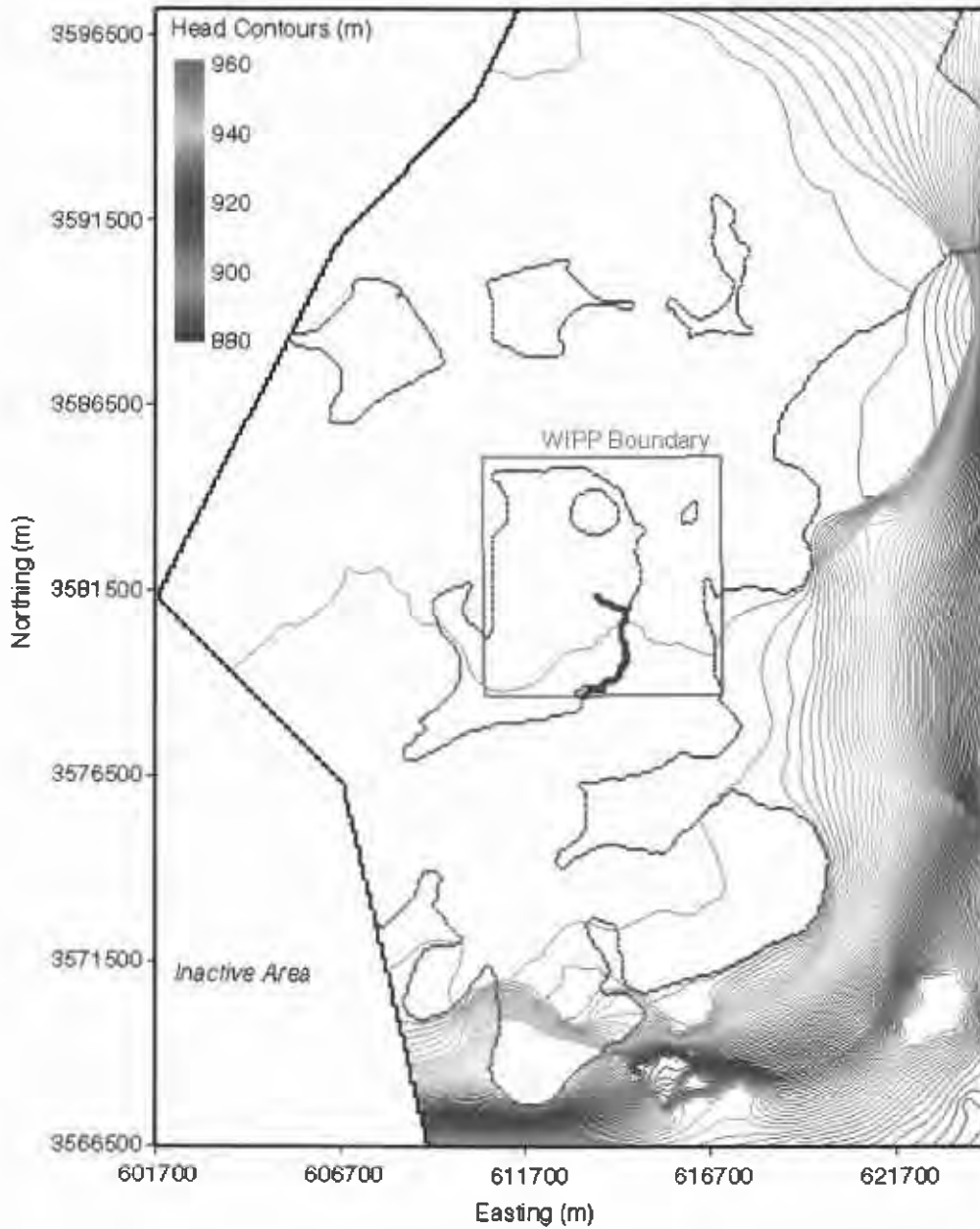


Figure 22: Head contours and particle track for the median travel time T-field (d12r08-R3) for the full-mining case. The WIPP boundary is the red box in the center of the figure and the particle track is the blue track originating from the approximate center of the WIPP.

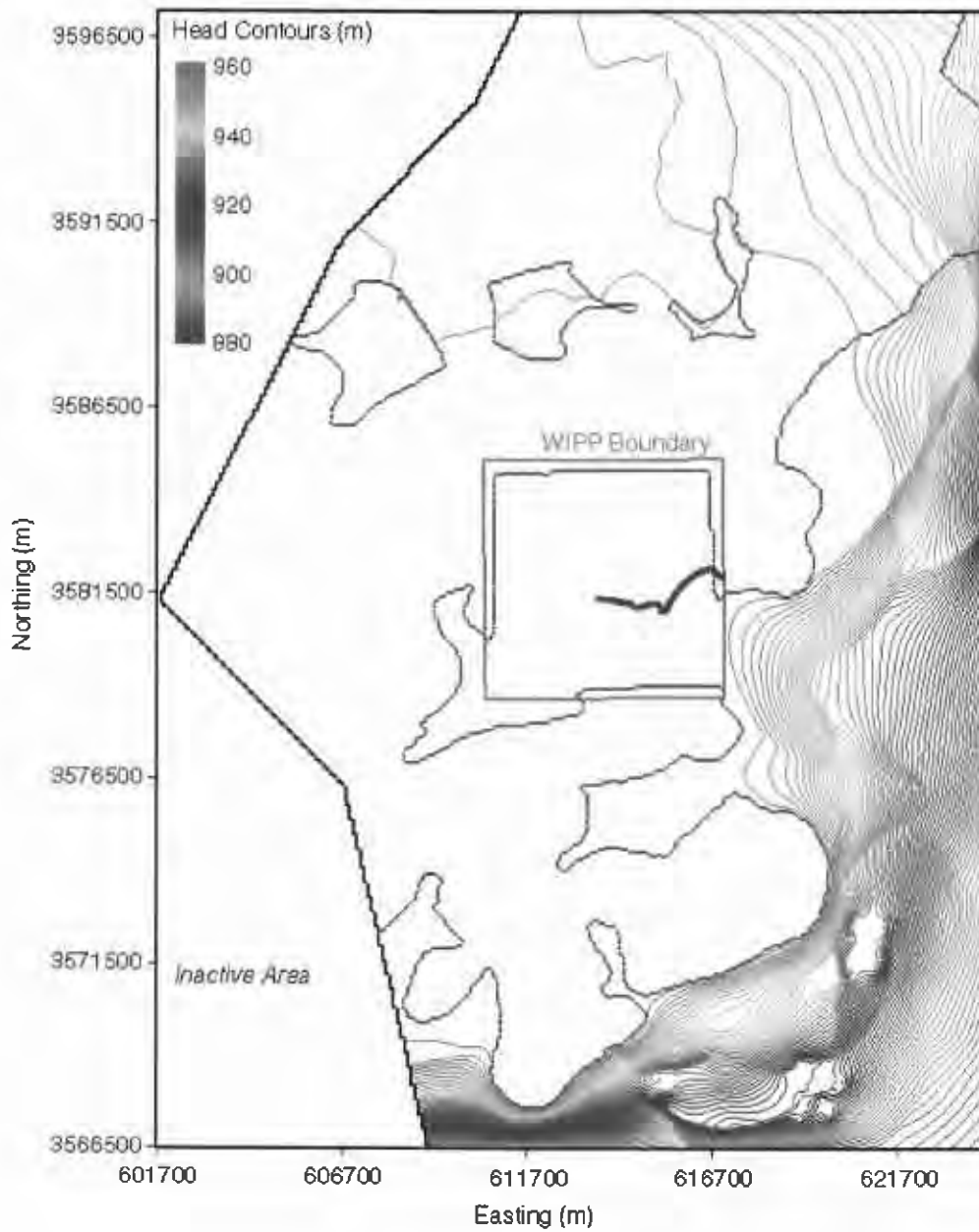


Figure 23: Head contours and particle track for the maximum travel time T-field (d03r01-R3) for the partial-mining case. The WIPP boundary is the red box in the center of the figure and the particle track is the blue track originating from the approximate center of the WIPP.

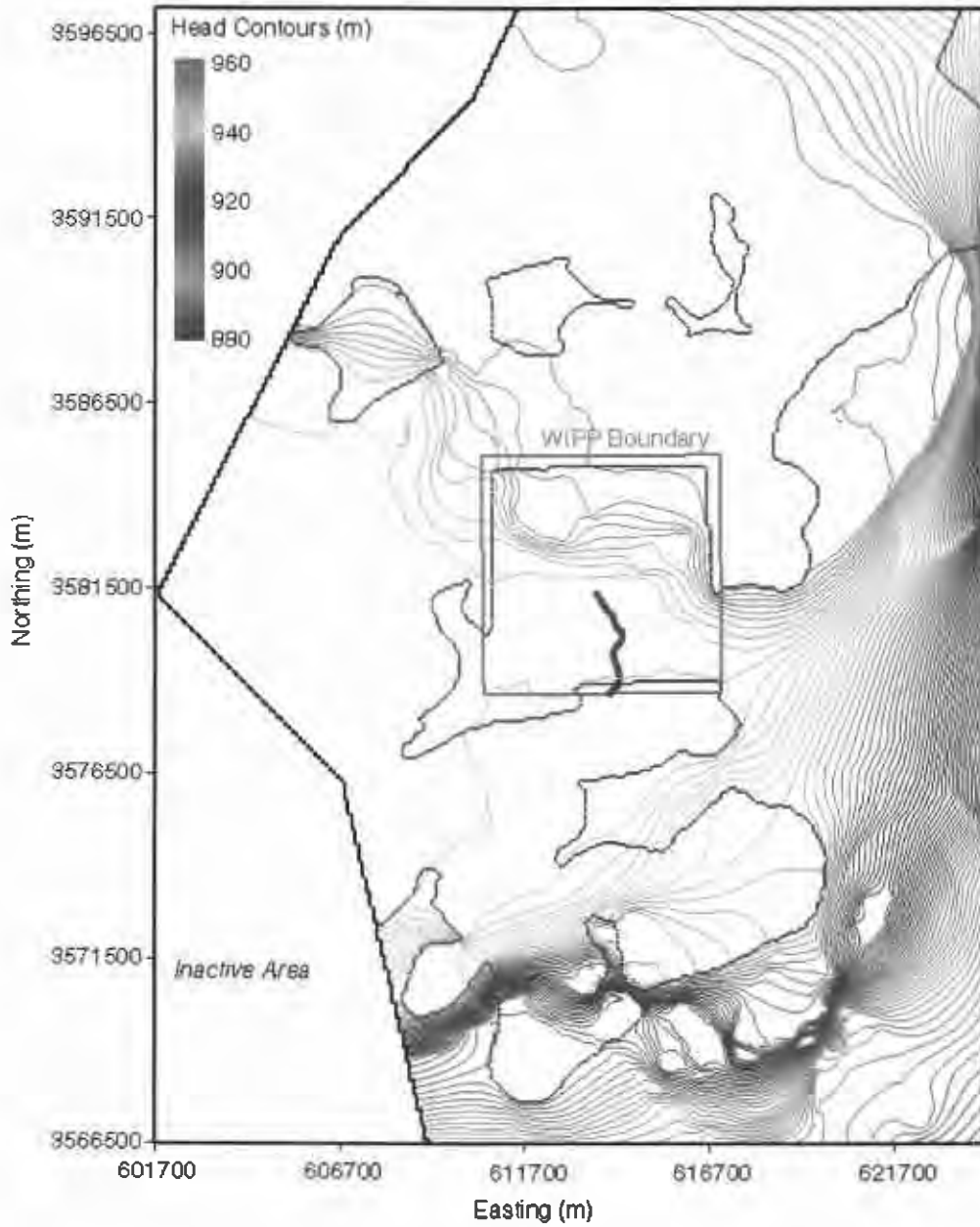


Figure 24: Head contours and particle track for the minimum travel time T-field (d09r06-R2) for the partial-mining case. The WIPP boundary is the red box in the center of the figure and the particle track is the blue track originating from the approximate center of the WIPP.

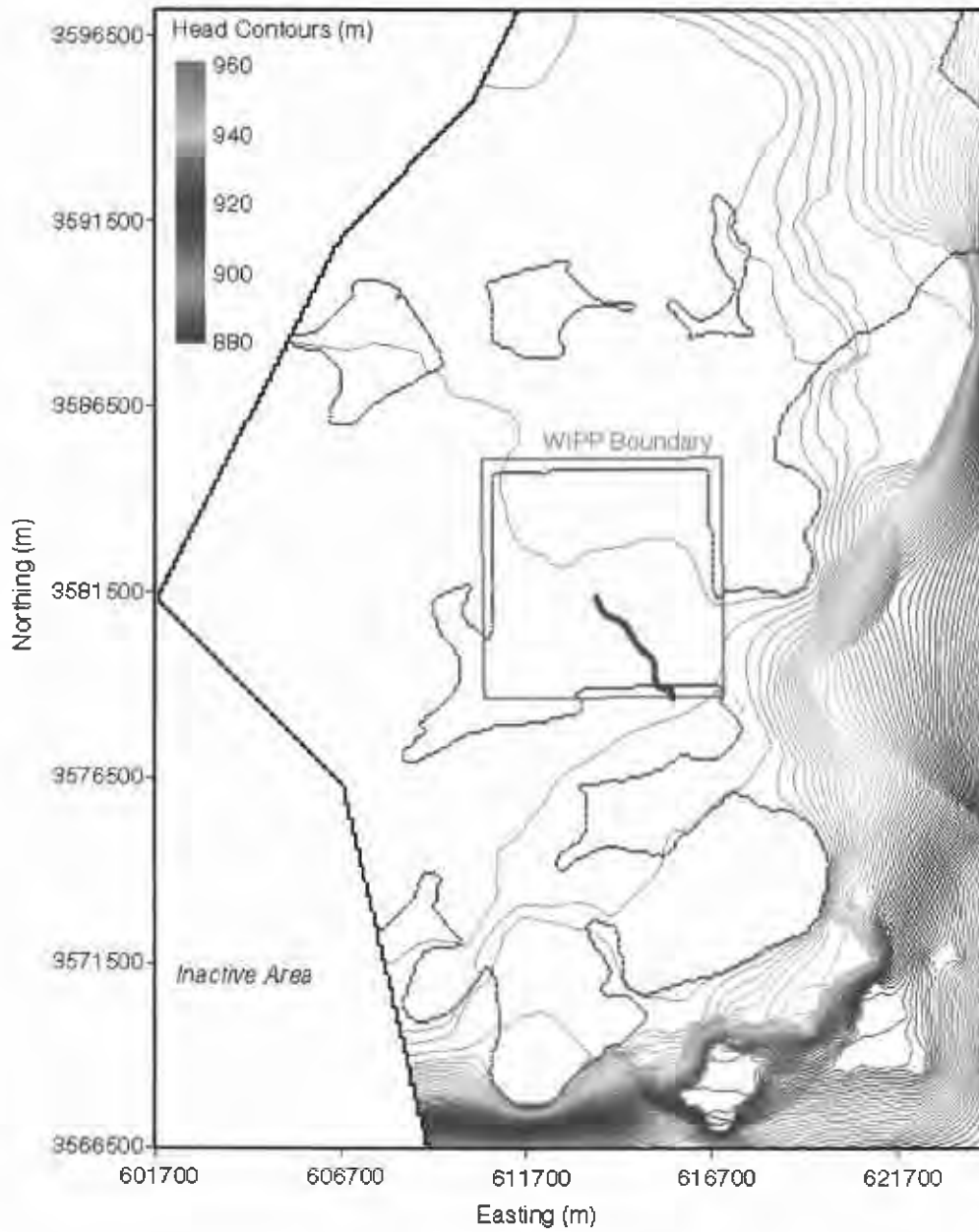


Figure 25: Head contours and particle track for the median travel time  $T$ -field (d13r07-R2) for the partial-mining case. The WIPP boundary is the red box in the center of the figure and the particle track is the blue track originating from the approximate center of the WIPP.

the 1996 CCA and the 2003 CRA (Lowry, 2003a). The CDF's describe the probability of a conservative tracer reaching the LWB at a given time. In addition to comparing travel times, particle tracking directions are also examined to determine the effect on the regional flow direction in the WIPP area due to mining. The flow fields generated from the mining scenarios are then refined and passed to Task 6 of AP-100 that performs radionuclide transport modeling in the Culebra.

Results show that for both the full- and partial-mining scenarios, the median particle travel times of 75,774 and 129,202 years are 4.14 and 7.06 times longer than for the non-mining scenario (18,289 years). The increase in transmissivity due to mining increases the relative flow rate through the mining zones, with a corresponding decrease in flow through the non-mining zones. This decrease in flow through the non-mining zones produces longer travel times for the mining scenarios. Comparing the full- mining scenarios of the CRA-revised analysis to the CCA and CRA calculations, the median travel times are approximately 2.53 and 1.14 times longer, respectively. For the partial mining case, the median travel time is 9.33 times greater than the median for the CCA, and 2.67 times greater than the CRA. This increase in the travel time over the CRA can be attributed to the higher percentage of area deemed as mining zone.

Unlike the CRA, a negative correlation was found in the CRA-revised analysis between the travel times and the random mining factor (the higher the random mining factor, the longer the particle travel time). This again is due to a higher percentage of mining zone area in the CRA-revised analysis as compared to the CRA. With a higher percentage of mining area, the random mining factor has a larger influence on the regional flow regime. As the mining factor is increased, the flow through the non-mining areas is decreased, producing longer travel times and the negative correlation. However, additional analysis shows that most of the travel time variability is due to differences in the base T-fields and not the random mining factor.

## References

- Beauheim, R. L., 2003. Analysis Report for AP-100 Task 1: Development and Application of Acceptance Criteria for Culebra Transmissivity (T) Fields. Carlsbad, NM: SNL, ERMS # 531136.
- BLM, 1993. Preliminary Map Showing Distribution of Potash Resources, Carlsbad Mining District, Eddy and Lea Counties, New Mexico. Roswell District, U.S. Bureau of Land Management (BLM).
- Cotsworth, E., 2004. Letter to R.P. Detwiler, Acting Manager, Carlsbad Field Office, U.S. Department of Energy from E. Cotsworth, Director, Office of Radiation and Indoor Air, U.S. Environmental Protection Agency, September 2, 2004. Copy on file in the Sandia WIPP Records Center, Carlsbad, NM, ERMS # 536711.
- GMS, 2003. Groundwater Modeling System: Developed by the Environmental Modeling Research Laboratory of Brigham Young University in partnership with the U.S. Army Engineer Waterways Experiment Station, Vicksburg, MS 39180. <http://chl.wes.army.mil/software/gms/default.htm>.
- Harbaugh, A. W., Banta, E., Hill, M. C., McDonald, M., 2000. MODFLOW 2000: The U.S. Geological Survey Modular Ground-Water Model - User Guide to Modularization Concepts and the Ground-Water Flow Process. U.S. Geological Survey, Reston, VA, open file report 00-92, 121pp.
- Holt, R. M., Yarbrough, L., 2003. Addendum 2 to Analysis Report, Task 2 of AP-088, Estimating Base Transmissivity Fields. ERMS #529416.
- Leigh, C., Beauheim, R. L., Kanney, J. F., 2003. Analysis Plan for Calculations of Culebra Flow and Transport: Compliance Recertification Application, AP-100, Revision 0. Carlsbad, NM: Sandia National Laboratories. ERMS # 530172.
- Lowry, T. S., 2003a. Analysis Report of Task 5 of AP-088, Evaluation of Mining Scenarios; Analysis Package for the Culebra Transport Calculations: Compliance Recertification Application. Carlsbad, NM: Sandia National Laboratories. ERMS # 530147.
- Lowry, T. S., 2003b. Analysis Report of Tasks 2 and 3 of AP-100, Grid Size Conversion and Generation of SECOTP2D Input; Analysis Package



- for Calculations of Culebra Flow and Transport: Compliance Recertification Application. Carlsbad, NM: Sandia National Laboratories. ERMS # 531137.
- McKenna, S. A., Hart, D., 2003a. Analysis Report, Task 3 of AP-088, Conditioning of Base T Fields to Steady-State Heads. Sandia National Laboratory. ERMS #529633.
- McKenna, S. A., Hart, D., 2003b. Analysis Report, Task 4 of AP-088, Conditioning of Base T Fields to Transient Heads. ERMS #531124.
- Ramsey, J., Wallace, M. G., Jow, H.-N., 1996. Analysis Package for the Culebra Flow and Transport Calculations (Task 3) of the Performance Assessment Analysis Supporting the Compliance Certification Application. Analysis Plan 019, Version 00, ERMS #240516.
- Rudeen, D. K., 2003. Users Manual for DTRKMF, Version 1.00. ERMS #523246. Carlsbad NM: Sandia National Laboratories, WIPP Records Center.
- Wallace, M. G., 1996. Record of FEP screening work, FEP ID# NS-11: Subsidence associated with mining inside or outside the controlled area. ERMS #240816.
- WIPP\_PA, 2003. WIPP PA Design Document for DTRKMF, Version 1.00. Sandia National Laboratories, ERMS #523244.

## Appendix A: Qualified Runs and Random Mining Factors

Qualified runs and random mining factors for each replicate (R1, R2, & R3).

Run #	R1	R2	R3
d01r02	905.50	32.85	13.54
d01r04	508.40	345.10	202.20
d01r07	340.30	996.50	936.30
d01r10	615.20	828.20	391.80
d02r02	575.30	579.30	306.80
d03r01	104.00	760.50	955.80
d03r03	94.06	514.90	77.79
d03r06	913.30	187.60	238.40
d03r07	630.50	567.10	725.20
d03r08	208.90	475.90	85.67
d03r09	769.30	750.00	647.80
d04r01	130.20	630.30	478.70
d04r02	351.90	453.30	996.70
d04r03	46.87	310.90	123.90
d04r04	194.60	487.90	217.30
d04r05	806.90	923.80	138.30
d04r06	264.40	584.00	835.30
d04r07	931.50	733.90	802.00
d04r08	897.90	51.08	96.80
d04r10	32.56	256.50	34.02
d05r03	394.10	108.30	159.00
d05r07	998.20	535.90	145.50
d06r02	790.00	679.40	826.70
d06r03	384.10	171.20	261.20
d06r04	258.50	860.00	293.90
d06r05	432.50	754.10	257.60
d06r06	10.02	653.20	172.50
d06r07	514.10	221.50	915.60
d06r10	282.90	70.11	861.40
d07r01	927.30	694.20	625.20
d07r02	691.30	864.90	737.80
d07r05	738.40	775.30	241.60
d07r06	450.20	591.70	548.70
d07r07	609.60	447.20	841.00
d07r08	557.70	942.30	349.00
d07r09	538.60	98.94	285.00
d07r10	713.60	379.60	187.30
d08r01	849.30	408.40	194.00
d08r02	569.70	989.10	893.90
d08r03	419.50	43.16	356.30
d08r04	160.00	834.00	857.00
d08r05	971.90	881.10	671.60
d08r06	118.80	558.90	743.20
d08r07	741.30	130.20	706.70
d09r02	729.70	497.00	429.30
d09r03	483.00	197.30	168.20
d09r04	580.60	661.30	766.40
d09r05	228.50	240.90	481.90
d09r06	474.10	383.50	449.10
d09r07	887.20	952.10	503.30

d09r08	66.07	339.80	327.30
d09r09	375.70	806.30	374.20
d09r10	521.10	906.90	24.83
d10r02	181.60	274.60	651.90
d10r03	298.50	796.60	816.70
d10r04	705.30	364.70	518.20
d10r06	84.20	819.40	690.80
d10r07	627.30	728.60	551.20
d10r08	403.20	414.80	670.30
d10r09	464.20	649.90	885.40
d10r10	821.40	607.80	925.70
d11r01	307.60	895.10	492.90
d11r02	236.50	918.30	364.50
d11r06	249.90	159.70	5.43
d11r07	543.50	86.78	966.70
d11r08	18.75	16.92	973.80
d11r09	215.40	618.30	576.30
d11r10	73.60	168.90	403.20
d12r01	317.40	683.30	756.20
d12r02	958.60	204.90	598.10
d12r03	686.00	322.00	333.80
d12r05	860.70	637.50	589.70
d12r06	363.80	359.00	56.05
d12r07	660.40	434.90	463.10
d12r08	940.20	708.20	312.10
d12r09	132.50	464.10	794.60
d13r01	983.00	971.30	901.70
d13r02	672.80	144.50	224.80
d13r03	643.20	849.00	415.20
d13r05	425.80	118.60	688.00
d13r06	961.10	785.90	385.40
d13r07	346.10	282.90	711.40
d13r08	838.60	78.26	64.98
d13r09	491.00	8.68	458.00
d21r01	755.40	307.30	632.40
d21r02	172.60	396.20	614.80
d21r03	591.50	422.30	46.61
d21r04	322.70	715.50	276.80
d21r05	855.70	870.90	105.80
d21r06	272.00	501.20	984.40
d21r07	652.50	296.70	940.20
d21r10	790.50	212.70	562.50
d22r02	163.20	527.50	870.60
d22r03	812.70	264.30	634.50
d22r04	144.70	140.70	526.30
d22r06	26.04	962.70	111.70
d22r07	870.30	548.10	609.10
d22r08	773.60	235.30	771.70
d22r09	53.04	937.70	784.10
d22r10	460.40	24.35	434.60